iScience

CellPress
OPEN ACCESS

Article

Genomic erosion and horizontal gene transfer shape functional differences of the ExlA toxin in *Pseudomonas* spp.

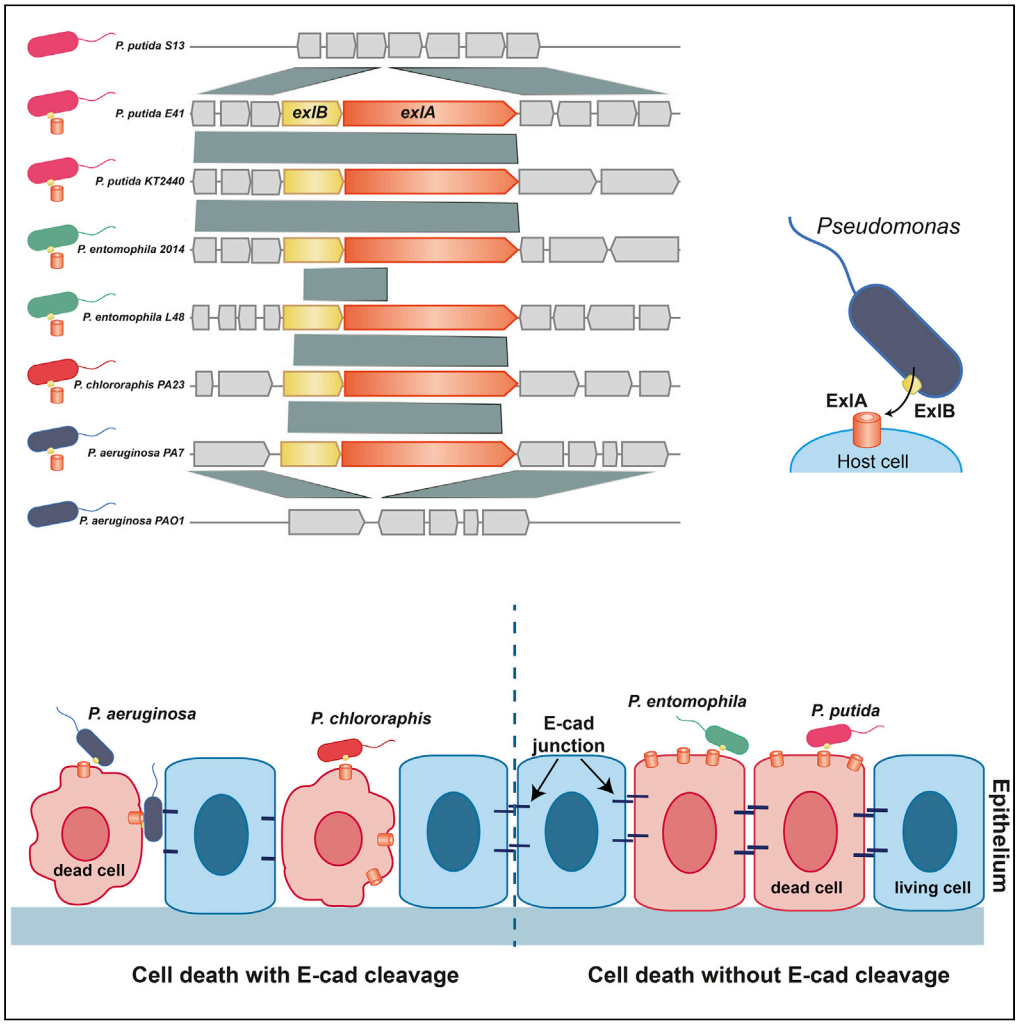

Viviana Job, Laura Gomez-Valero, Adèle Renier, ..., Yohann Couté, Carmen Buchrieser, Ina Attrée

cbuch@pasteur.fr (C.B.)
ina.attree@ibs.fr (I.A.)

Highlights

ExlA is a two-partner secreted toxin conserved across *Pseudomonas* spp.

Environmental *Pseudomonas* strains encode ExlA with different cytotoxic activities

ExlA of environmental *Pseudomonas* strains play a role in bacteria-insect interactions

ExlBA operon shows a complex evolutionary history of horizontal gene transfer

Job et al., iScience *25*, 104596
July 15, 2022
https://doi.org/10.1016/j.isci.2022.104596

iScience

CellPress
OPEN ACCESS

Article

Genomic erosion and horizontal gene transfer shape functional differences of the ExlA toxin in *Pseudomonas* spp.

Viviana Job,[1] Laura Gomez-Valero,[2] Adèle Renier,[1] Christophe Rusniok,[2] Stephanie Bouillot,[1] Viviane Chenal-Francisque,[2] Erwan Gueguen,[3] Annie Adrait,[4] Mylène Robert-Genthon,[1] Katy Jeannot,[6] Peter Panchev,[1] Sylvie Elsen,[1] Marie-Odile Fauvarque,[4] Yohann Couté,[4,5] Carmen Buchrieser,[2,*] and Ina Attrée[1,7,*]

SUMMARY

Two-partner secretion (TPS) is widespread in the bacterial world. The pore-forming TPS toxin ExlA of *Pseudomonas aeruginosa* is conserved in pathogenic and environmental *Pseudomonas*. While *P. chlororaphis* and *P. entomophila* displayed ExlA-dependent killing, *P. putida* did not cause damage to eukaryotic cells. ExlA proteins interacted with epithelial cell membranes; however, only ExlA^{Pch} induced the cleavage of the adhesive molecule E-cadherin. ExlA proteins participated in insecticidal activity toward the larvae of *Galleria mellonella* and the fly *Drosophila melanogaster*. Evolutionary analyses demonstrated that the differences in the C-terminal domains are partly due to horizontal movements of the operon within the genus *Pseudomonas*. Reconstruction of the evolutionary history revealed the complex horizontal acquisitions. Together, our results provide evidence that conserved TPS toxins in environmental *Pseudomonas* play a role in bacteria-insect interactions and discrete differences in CTDs may determine their specificity and mode of action toward eukaryotic cells.

INTRODUCTION

Bacterial evolution is largely driven by horizontal gene transfer (HGT) between populations thriving in the same habitats (Gomez-Valero and Buchrieser, 2019; Koonin, 2016). Bacteria from the genus *Pseudomonas* are ubiquitous on earth because of their extraordinary capacities to adapt to diverse niches. *Pseudomonas* species are associated with plants and animals and are frequently found in the proximity of human activities (Silby et al., 2011). *Pseudomonas aeruginosa* is a human opportunistic pathogen that causes high-cost health problems notably due to the increasing number of multi-drug resistant strains. The World Health Organization [WHO] classified carbapenem-resistant *P. aeruginosa* in the high-priority category of bacterial pathogens for which there is an urgent need to define new antimicrobials (Organization, 2019). In addition to a panoply of surface-attached and exported virulence factors, some clinical *P. aeruginosa* strains use a pore-forming toxin Exolysin (ExlA^{Pa}) for efficient host cell destruction and infectivity (Elsen et al., 2014; Reboud et al., 2016). *ExlA*-positive *P. aeruginosa* represents around 2% of the strains present in clinical cohorts and is more frequent in aquatic environments (Reboud et al., 2016; Wiehlmann et al., 2015). Examination of the genetic environment of *exlA* homologs identified in different *Pseudomonas* species and their species-specific regulation led to a speculation that the operon has been acquired through HGT (Trouillon et al., 2020).

ExlA is exported by a cognate outer-membrane transporter, ExlB (Basso et al., 2017), and the two proteins belong to a two-partner secretion (TPS) system, also known as a type 5b secretion system (T5bSS) (Guerin et al., 2017; Nash and Cotter, 2019a, 2019b). ExlA shares the common TpsA domain architecture (Guerin et al., 2017), comprising Sec and TPS signals at the N-terminal part of the protein, central repeated filamentous hemagglutinin domains (FHA), and a C-terminal domain (CTD) that carries the activity. ExlB contains the conserved "loop 6" of the Omp85 family defined by the conserved arginine and aspartate of the (V/I)RG(Y/F) and (G/F)xDxG motifs of the FhaC family of TpsB proteins (Yeo et al., 2007; Maier et al., 2015). Based on the molecular studies of model systems, TpsA and TpsB proteins are first translocated across the cytoplasmic membrane to the periplasm by the Sec secretion system.

[1]Université Grenoble Alpes, Institute of Structural Biology, Bacterial Pathogenesis and Cellular Responses Team, UMR5075 CNRS, IRIG, CEA, Grenoble, France

[2]Institut Pasteur, Université de Paris, CNRS UMR 6047, Unité Biologie des Bactéries Intracellulaires, 75015 Paris, France

[3]University of Lyon, Université Lyon 1, INSA de Lyon, CNRS UMR 5240 Microbiologie Adaptation et Pathogénie, Lyon, France

[4]Université Grenoble Alpes, INSERM, CEA, UMR BioSanté U1292, Grenoble, France

[5]CNRS, CEA, FR2048, Grenoble, France

[6]Centre National de Référence de la Résistance aux Antibiotiques, Laboratoire de Bactériologie, Centre Hospitalier Universitaire Jean Minjoz, UMR6249 CNRS, Université de Bourgogne-Franche Comté, Besançon, France

[7]Lead contact

*Correspondence: cbuch@pasteur.fr (C.B.), ina.attree@ibs.fr (I.A.)

https://doi.org/10.1016/j.isci.2022.104596

There, TpsB is inserted into the outer membrane and forms a β-barrel that has channel activity. TpsA remains in an extended conformation in the periplasm and interacts with periplasmic chaperones (Baud et al., 2009; Johnson et al., 2021) and with the two periplasmic POTRA domains of its TpsB partner (Delattre et al., 2011; ur Rahman et al., 2014), which opens the pore and starts the translocation of TpsA across the outer membrane. Once it reaches the cell surface, TpsA starts to fold into a β-helix and the TPS domain is thought to initiate the folding (Jacob-Dubuisson et al., 2004; Nash and Cotter, 2019a, 2019b). TpsA proteins have different activities and are classified in families of adhesins, proteases, contact-dependent growth inhibition proteins (Cdi), and cytolysins/hemolysins. ExlA belongs to the cytolysin/hemolysin family, with ShlA of *Serratia marcescens*, HmpA of *Proteus mirabilis*, EthA of *Edwardsiella tarda*, or HhdA of *Haemophilus ducreyi* as representatives (Guerin et al., 2017; Jacob-Dubuisson et al., 2013).

The three-dimensional structures of the TPS and FHA domains have been reported for several TpsA proteins of different classes (Clantin et al., 2004; Guerin et al., 2017; Weaver et al., 2009; Yeo et al., 2007; Zambolin et al., 2016). The *P. aeruginosa* ExlA (ExlA^{Pa}) CTD folds in a so-called molten globule without any recognized structural features. The "molten globule" fold was proposed to facilitate the incorporation of the protein in the host lipid bilayer where it forms a pore of defined size (Bertrand et al., 2020; Faudry et al., 2007). The consequences of the pore formation are immediate influx of Ca^{2+} ions within the host cytoplasm and the activation of the host metalloprotease ADAM10, which in turn cleaves the main cell-cell junction protein E-cadherin (Maretzky et al., 2005). *In vivo*, the ExlA-dependent cleavage of E-cadherin results in bacterial dissemination and hemorrhagic pneumonia (Bouillot et al., 2020; Elsen et al., 2014). The presence of *exlBA*-like operons in *Pseudomonas* species other than *P. aeruginosa* that are non-pathogenic for humans suggested that this TPS may play a role in the infection of other organisms, prokaryotes or eukaryotes, as it was recently suggested for *Pseudomonas protegens* (Vesga et al., 2020).

Here, we examined 191 ExlA sequences retrieved from publicly available databases. The overall amino acid sequence identity of proteins was distributed unevenly throughout the protein sequences. Furthermore, the subclass of ExlA proteins present in the natural fly pathogen *P. entomophila* (ExlA^{Pe}) and other soil-dwelling *Pseudomonas* exhibited CTDs that were shorter and differed in sequence compared to the ExlA^{P} class. The analyses of the expression and functionality of ExlA homologs in strains of *P. chlororaphis* (ExlA^{Pc}), *P. putida* (ExlA^{Pp}), and *P. entomophila* (ExlA^{Pe}) and their comparison with the well-characterized *P. aeruginosa* ExlA identified similarities and differences between their structures and activities *in vitro* toward the eukaryotic cells and *in vivo* in infection of their specific hosts. Comparative genomics and phylogenetic analyses allowed to gain insight in the origin and evolution of these genes in the different *Pseudomonas* species.

RESULTS

TPS exolysins display divergent CTDs across *Pseudomonas* species

Our previous study analyzing the promotor sequences and regulation of the *exlBA* operon identified *exlBA* sequences in 466 *Pseudomonas* strains among the over 4,800 *Pseudomonas* strains present in the *Pseudomonas* database (Trouillon et al., 2020). This intriguing finding led us to investigate here the sequences and the function of the corresponding proteins in selected, commonly used strains of the species *P. entomophila*, *P. putida*, and *P. chlororaphis* that can be genetically manipulated. Interestingly, although the sequence of the overall ExlA protein is conserved in all species, it differs among domains. The TPS domain is 82% conserved, whereas the FHA domains are only 34% conserved and exhibit two different regions in which indels are present. The highest divergence is present in the CTDs as they are only 9% conserved (Figure 1A). Importantly, the ExlA^{Pp}-CTD lacks 118 residues compared to the CTDs from its homologs in *P. aeruginosa* and *P. chlororaphis* (Figures 1B and S1), due to a fragment missing inside the CTD of *P. putida* strains. Similarly, a deletion is present in strains of the species *Pseudomonas parafulva* and *Pseudomonas rhizosphaerae* (Figure S2). In *P. entomophila* strains, the ExlA^{Pe}-CTD is even shorter as it comprises only 121 or 168 residues in strains L48 and 2014/1257, respectively, compared to 287 amino acids for the CTDs in *P. aeruginosa* and *P. chlororaphis* PA23. Despite the difference in sequence conservation, the global conservation of the exporters TpsB/ExlB (between 42 and 69% identity) in the four species studied within this work is considerably higher than that of the exported protein TpsA/ExlA (Figure 1C and Table S4), suggesting that, while the TPS export is conserved, the substrates may have evolved to perform different activities.

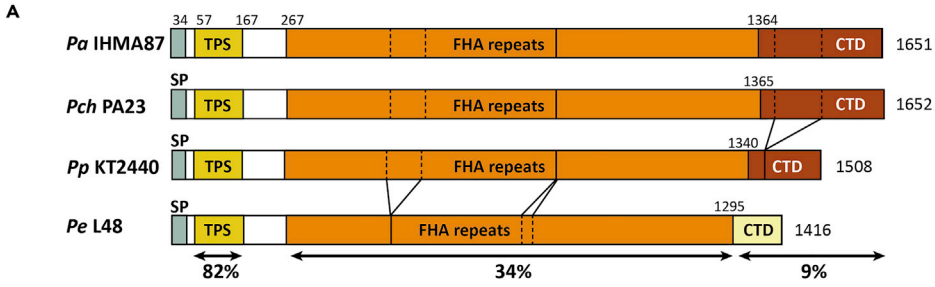

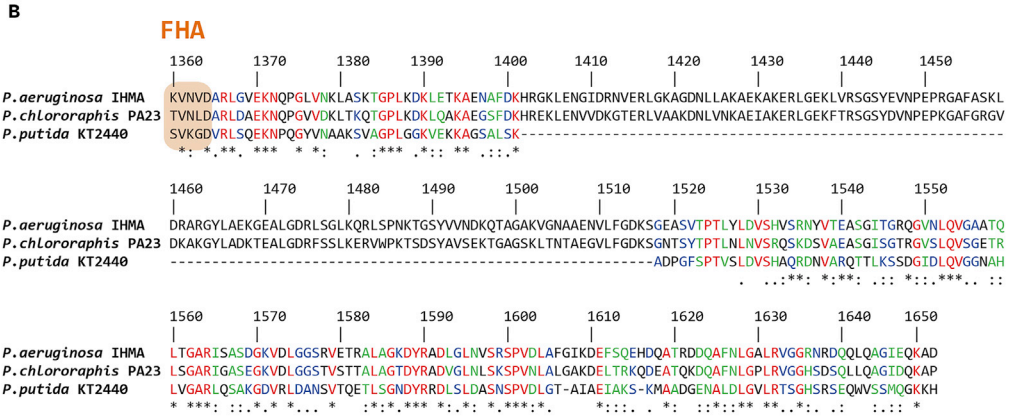

C

	Pa IHMA87	*Pch* PA23	*Pp* KT2440	*Pe* L48
Pa IHMA87	*	62.08%	40.98%	46.32%
Pch PA23	67.71%	*	39.92%	54.02%
Pp KT2440	44.03%	41.98%	*	34.74%
Pe L48	65.43%	68.93%	42.23%	*

ExlA
ExlB

Figure 1. Conservation of ExlA-like proteins in different *Pseudomonas* species

(A) Domain arrangement of ExlA proteins in indicated bacteria. The numbering of amino acids corresponding to each protein domain is shown. SP, signal peptide; TPS, two-partner secretion domain; FHA, filamentous hemagglutinin repeats; CTD, C-terminal domain. Amino acid identity between domains are shown in %.

(B) Alignments of two types of ExlA CTDs: ExlA from *P. aeruginosa* IHMA87, *P. chlororaphis* PA23 and *P. putida* KT2440 (upper panel) and ExlA from *P. entomophila* L48 and ExlA from soil-*Pseudomonas* species (bottom panel). The end of the last predicted FHA is indicated in orange box. Note the large deletion within the CTD of the ExlA^{Pp} protein. The alignment of entire proteins from the four species studied is presented in Figure S1.

(C) Amino acid identity (%) of ExlA (in orange) and ExlB (in yellow) proteins between different *Pseudomonas* spp. See also Figure S1 and Table S4.

Eukaryotic cells are sensitive to ExlA-like proteins from various *Pseudomonas* species

Virulent clinical isolates of *P. aeruginosa* secreting ExlA^{Pa} display cytotoxicity for a variety of eukaryotic cells by forming pores in the host plasma membrane, leading to altered K^+ and Ca^{2+} signaling, cleavage of cell-cell junctions, and cell death (Basso et al., 2017; Reboud et al., 2017). To assess whether orthologs of ExlA^{Pa} in *P. chlororaphis*, *P. entomophila*, and *P. putida* are also able to provoke the eukaryotic cell death, we co-incubated these different strains with A549 or J774 cells and measured the kinetics of incorporation of the membrane-impermeable dye propidium iodide (PI) into DNA using the fluorescence emission at 590 nm as a read-out for cytotoxicity (Figure 2). First, we tested several *P. chlororaphis* strains isolated from diverse environments (Key resources table and Figure S4). All displayed comparable levels and kinetics of cytotoxicity on both cell types, similar to what has been reported for the reference strain *P. chlororaphis* PA23 for which cytotoxicity has been shown to be ExlB-ExlA dependent (Trouillon et al., 2020). No significant difference in the levels of cytotoxicity was observed between human and environmental isolates. The protein content of secretomes of three *P. chlororaphis* strains, using mass spectrometry (MS)-based quantitative

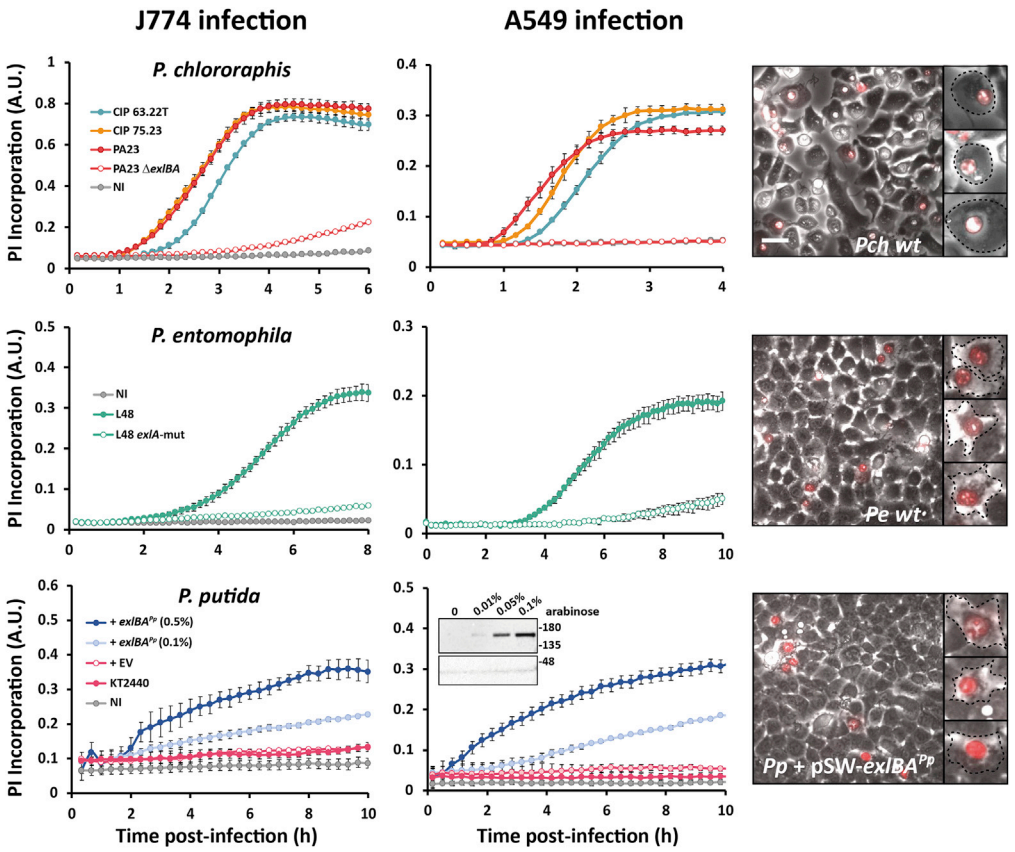

Figure 2. Cytotoxicity of various *Pseudomonas* strains on eukaryotic cells is ExlA-dependent

Cytotoxicity profiles on epithelial A549 cells and J774 macrophages of *P. chlororaphis* PA23, *P. entomophila* L48, and *P. putida* KT2440 overexpressing *exlBA in trans* in pSW vector. Murine macrophages (J774, left panel) and epithelial cells (A549, middle and right panels) were infected at an MOI of 10 at 30°C with different strains, as indicated. Cell death was monitored by PI incorporation. Fluorescence emission at 590 nm, expressed as arbitrary units (A.U.), was recorded over indicated time post-infection (h). Immunoblot of secreted ExlA^{Pp} induced with different concentrations of arabinose and detected by anti-ExlA^{Pa} antibodies are shown in the inner panel with loading controls (an unspecific western blot signal for *P. putida* KT2440). Microscopy images (right panel) were taken after 2 h of infections with *P. chlororaphis* PA23 (*Pch wt*) or 4 h of infection with *P. entomophila* L48 (*Pe wt*) and *P. putida* KT2440 expressing *exlBA in trans* (*Pp* + pSW-*exlBA*^{Pp}) in presence of 0.1% arabinose. One representative superposed image of transmission and PI-fluorescence is shown for each bacterium, with zoom on several selected cells showing incorporation of PI. To note, the A549 cells infected by *P. chlororaphis* lost cell-cell contacts. On the other hand, the A549 cells infected by *P. entomophila* and *P. putida* + *exlA*^{Pp} kept their initial shape while having incorporated the PI within the nuclei. Scale bar represents 50 μm. Each experiment was repeated at least three times. The representative graphs are issued from four technical replicates; means are calculated and presented with corresponding standard deviation. See also Figures S3–S5, Table S2 and Table S3.

proteomics, showed that *P. chlororaphis* CIP63 and *P. chlororaphis* CIP75, like the reference strain *P. chlororaphis* PA23, secrete the ExlA homologs in culture supernatants (Figure S3A and Table S2). Of note, *P. chlororaphis* CIP63 secreted less ExlA, which correlated with a slightly lower cytotoxicity (Figure 2).

P. entomophila L48 is widely studied in the context of host-pathogen interactions using *Drosophila* flies (Liehl et al., 2006; Vodovar et al., 2005, 2006). It secretes three main virulence factors regulated by the global GacS/GacA two-component regulatory system: the pore-forming toxin Monalysin, the protease AprA, and the hemolytic Entolysin A, all contributing to the bacterial invasion and/or killing of the host (Opota et al., 2011; Vallet-Gely et al., 2010b; Vodovar et al., 2005). To study the role of ExlA in eukaryotic cell lysis without interference of Monalysin, the principal virulence factor, we inactivated *P. entomophila exlA* in a Δ*mnl* and Δ*gacA* background (Opota et al., 2011). As for *P. chlororaphis*, the secretome produced by these different *P. entomophila* mutant strains was characterized by MS-based quantitative proteomics, and the relative abundances of secreted proteins in each strain and between strains were compared (Figure S3B and

Table S3). These results confirmed that ExlA^{Pe} and Monalysin were both synthesized and secreted independently and that GacA had no influence on ExlA^{Pe} abundance as judged from the secretome. The kinetics of cytotoxicity on epithelial cells and macrophages of *P. entomophila* strains were delayed compared to that observed with *P. chlororaphis* or *P. aeruginosa* strains. However, in all three genetic backgrounds (wild-type, Δ*mnl*, Δ*gacA*), deficiency of ExlA abolished the capacity of the strains to induce necrosis of the eukaryotic cell (Figures 2 and S4).

We then tested a collection of strains belonging to the *P. putida* complex (Key resources table and Figure S4), including the reference strain KT2440 which harbors the *exlBA* operon. None of the strains, including KT2440, was cytotoxic, except one that was identified as *P. mosselii* (185886). To be able to study the activity of the ExlA homolog in *P. putida* KT2440, we expressed the *exlBA* operon (*PP_1449-PP_1450*) from the arabinose-inducible promoter. Upon induction by arabinose, ExlA^{Pp} was readily detected in bacterial culture supernatants using antibodies raised against ExlA^{Pa} (Figure 2 inset), and the cytotoxicity toward macrophages and epithelial cells increased with higher arabinose concentrations (Figure 2).

Microscopy analyses revealed different morphological changes on A549 cells during the infection with these four species. Although *P. aeruginosa*- and *P. chlororaphis*-infected cells that were PI positive detached from each other and rounded up, the cell layer infected by *P. entomophila* or *P. putida* looked intact and kept the cell-cell contact, despite the presence of PI-positive cells (Figures 2 and S5). Together, these results revealed that all four ExlA proteins cause permeability of eukaryotic cell membranes, but the mechanism leading to cell death seems different for *P. entomophila* and *P. putida* compared to *P. aeruginosa* and *P. chlororaphis*.

ExlA proteins display different activities toward membranes and E-cadherin

As ExlA^{Pa} is a membrane pore-forming toxin that binds to liposomes and host membranes (Basso et al., 2017; Bertrand et al., 2020), we tested whether the ExlA homologs can also be detected within infected cell membranes. In particular, we analyzed the detergent-resistant membrane (DRM) fractions called lipid rafts, enriched in cholesterol and sphingolipids, which are involved in protein sorting, signaling, and trafficking (Simons and Vintiner, 2011; Simons and Gerl, 2010). Membranes of infected human epithelial cells were separated using a sucrose density gradient centrifugation and the fractions were tested for the presence of ExlA proteins by immunoblotting. ExlA^{Pch} and ExlA^{Pa} were recovered only in the DRM fractions containing the lipid raft marker flotillin-2 (Figure 3A), demonstrating interactions and affinities toward host lipids similar to *P. aeruginosa*. In contrast, ExlA^{Pp} seems to be able to bind both DRM and detergent-soluble membranes (DSM) with a preference for DSM. Surprisingly, ExlA^{Pe} did not co-fractionate with DRM but was recovered in fractions containing DSM and cytoplasmic content (Figure 3A). To further investigate the localization of ExlA^{Pe} during infection, we labeled host surface proteins with biotin and purified the labeled proteins using NeutrAvidin Agarose beads. This strategy allowed us to show that ExlA^{Pe} co-eluted with the marker of membrane fractions, indicating that all four ExlA proteins are associated with eukaryotic membranes (Figures 3B and S6).

The cleavage of the cell-cell junction protein E-cadherin is a hallmark of cellular perturbations caused by the ExlA^{Pa} toxin upon activation of the host protease ADAM10 by Ca^{2+} influx (Reboud et al., 2017). ExlA^{Pch} also induced the cleavage of E-cadherin, producing a soluble C-terminal fragment of 30 kDa (Figures 3A and S6). Interestingly, neither ExlA^{Pp} nor ExlA^{Pe} induced E-cadherin cleavage. The fact that E-cadherin stays intact upon infection by *P. entomophila* L48 or *P. putida* KT2440 is in agreement with the observation that despite the detection of PI within the cell nuclei there is a conservation of A549 cell-cell adhesion contacts (Figure 2).

Therefore, ExlA^{Pe} has the capacity to associate with epithelial membranes, but its membrane anchor/interaction seems to be different compared to the three other *Pseudomonas* ExlA proteins that bind the lipid rafts. As neither *P. entomophila* L48 nor *P. putida* KT2440 expressing ExlA^{Pp} induce the E-cadherin cleavage, we concluded that lipid raft association and E-cadherin cleavage are independent events.

Contribution of CTDs to toxin activity

In different classes of TpsA proteins and in many polymorphic toxins (Zhang et al., 2012), the functional domain is located at the C-terminal part of the protein. Indeed, the ExlA^{Pa} CTD harbors the pore-forming activity (Basso et al., 2017). Considering the divergent sequences of the CTDs of ExlA^{Pa}/ExlA^{Pch}, ExlA^{Pp},

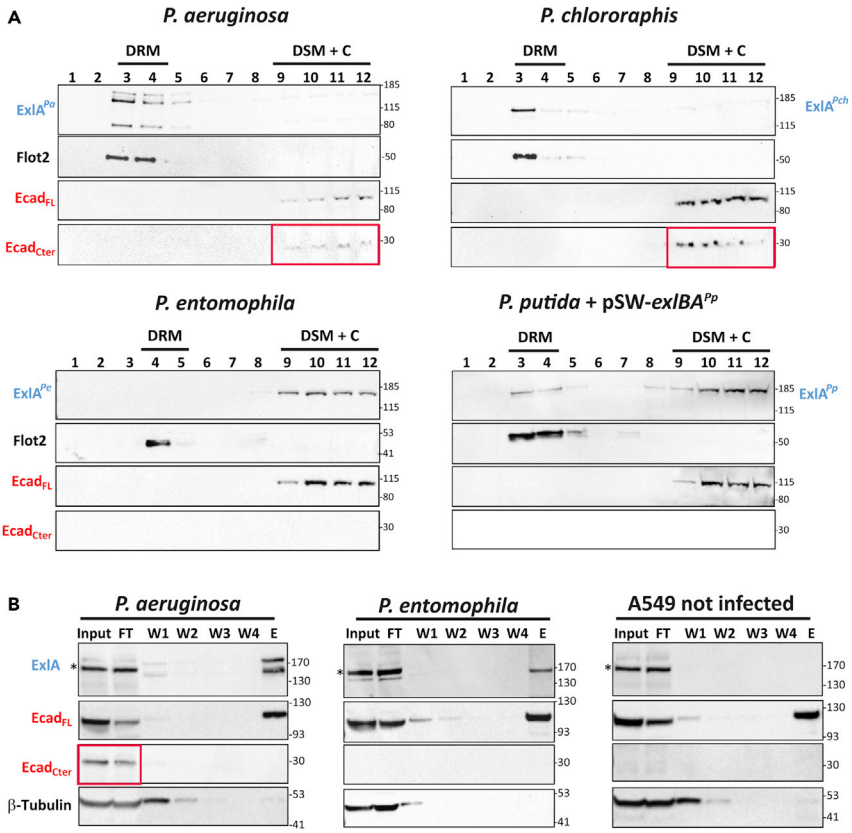

Figure 3. Association of ExlA proteins with lipid rafts and cleavage of E-cadherin

(A) Sucrose gradient fractions of infected epithelial cell membranes. Epithelial cells (A549) were infected with *P. chlororaphis* PA23, *P. entomophila* L48, *P. putida* KT2440 carrying pSW196-*exlBA*^{Pp}, and *P. aeruginosa* IHMA87, used here as positive control. Detergent-resistant membranes (DRM) containing lipid rafts were separated on sucrose gradient from the detergent-soluble membranes (DSM) and the cytoplasm (C), as described in STAR Methods. Protein contents of each fraction were separated on a gradient 4-12% acrylamide gel and analyzed by Western blotting using anti-ExlA^{Pa} antibodies. Anti-Flotillin-2 antibodies were used to localize lipid raft fractions. Anti-E-cadherin antibodies were used to assess the cleavage of the protein (full length, FL, and cleaved C-terminal fragment 30-kDa, Cter). Note that the *P. entomophila* ExlA does not co-fractionate with DRMs. Both *P. aeruginosa* and *P. chlororaphis* ExlAs induced the E-cadherin cleavage (highlighted in red boxes). Numbers on the top refer to the 12 fractions recovered from the top to the bottom of the tubes containing sucrose gradient, while sizes of protein markers in kDa are shown on the right.

(B) Affinity purifications of whole plasma membrane-bound protein contents using surface biotinylation. After 2-3 h of infections with *P. entomophila* or *P. aeruginosa*, used as positive control, the samples were biotinylated, and the whole lysates were subjected to affinity purification on avidin resin. The fractions from different purification steps were analyzed by Western blots using anti-ExlA^{Pa} antibodies, anti-E-cadherin antibodies as membrane control and anti-β-tubulin as cytoplasm control. Not infected A549 cells were treated in parallel. Input, cell lysate; FT, flow through; W, four washing steps; E, elution. *Non-specific signal revealed by the anti-ExlA^{Pa} antibodies. Note the presence of *P. entomophila* ExlA together with full-length E-cadherin within membranes, and absence of soluble cleaved C-terminal fragment, readily detected in sample from *P. aeruginosa* infection. See also Figure S6.

and ExlA^{Pe}, we hypothesized that the difference between the protein families in the affinity and activity toward membranes depends on their CTDs. To investigate their structure-function relationship, we designed chimeras with switched CTDs ExlA$^{Pa\text{Nter-}Pe\text{CTD}}$, ExlA$^{Pa\text{Nter-}Pp\text{CTD}}$, ExlA$^{Pe\text{Nter-}Pa\text{CTD}}$, and ExlA$^{Pe\text{Nter-}Pp\text{CTD}}$ (Figure 4A), and introduced them into two host strains: *P. aeruginosa* IHMA87 Δ*exlBA* and *P. entomophila* L48 Δ*exlBA*. We used ExlA$^{Pa-\text{Nter}}$ previously described (Bertrand et al., 2020) and engineered the *P. entomophila* protein lacking the CTD (ExlA$^{Pe-\text{Nter}}$) (Key resources table and Table S1) as controls. All chimeric proteins were synthetized and secreted at similar levels in the two bacterial backgrounds (Figure 4B inset). We then assessed the cytotoxicity of the chimeras on A549 cells. ExlA$^{Pa-\text{Nter}}$ was non-cytotoxic toward epithelial cells as previously reported (Basso et al., 2017), yet both chimeras carrying CTDs of *P. entomophila* or *P. putida* proteins restored the cytotoxicity, showing that the amino acid sequence

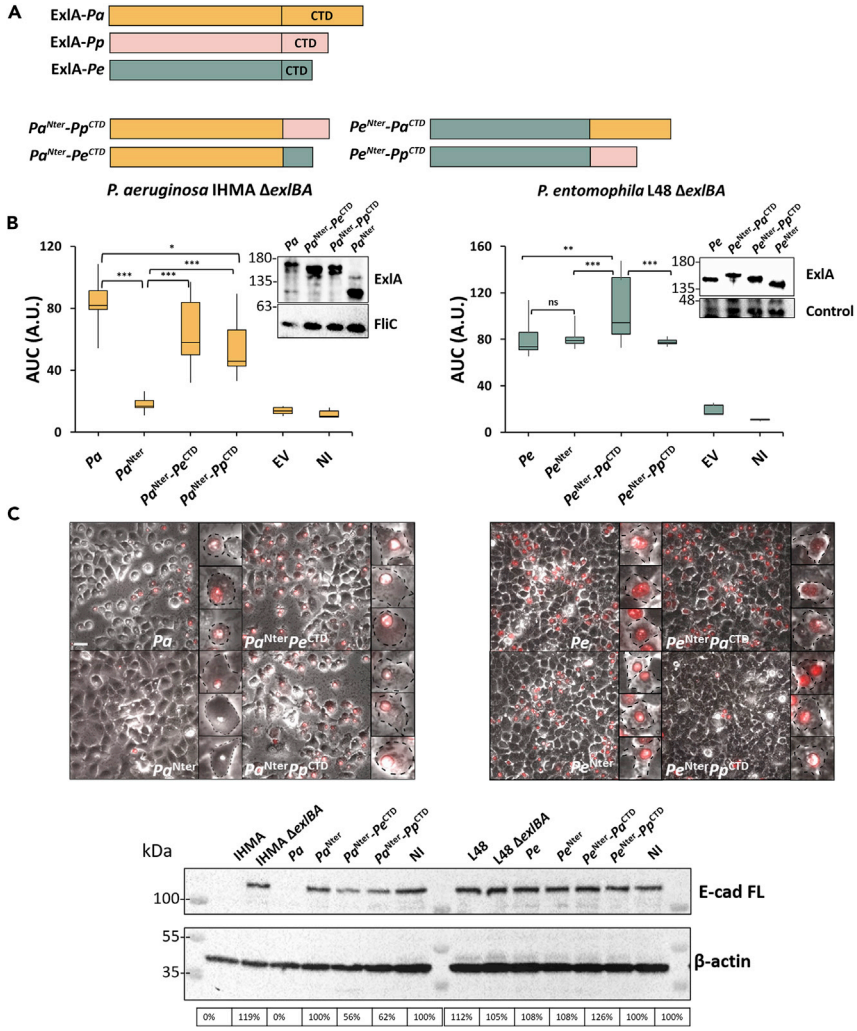

Figure 4. Contribution of different protein domains to ExlA function

(A) Schematic representation of chimeric proteins with switched CTDs.

(B) Comparison of cytotoxicity on epithelial A549 cells of *P. aeruginosa* IHMA Δ*exlBA* and *P. entomophila* L48 Δ*exlBA* expressing different chimeric proteins. Epithelial cells were infected at an MOI of 10 at 37°C without arabinose for *P. aeruginosa* and at 30°C in the presence of 0.01% arabinose for *P. entomophila*. PI incorporation was measured as fluorescence emission at 590 nm. AUCs were calculated according to the linear trapezoidal rule and are expressed in arbitrary unit. One-way ANOVA followed by a Holm-Sidak test was performed to determine statistically significant difference. $p \leq 0.05$ (*), $p \leq 0.01$ (**), $p \leq 0.001$ (***), ns: not significant. Cytotoxicity was followed for each strain at least three times in triplicates. Box plots show the median and standard deviation values.

(C) Microscopy images were taken during the infections with *P. aeruginosa* IHMA wild-type, IHMA Δ*exlBA* expressing *exlBA*^{Pa} (*Pa*), *exlBA*$^{Pa-Nter}$ (*Pa*^{Nter}) and the chimeric proteins (*Pa*^{Nter}-*Pe*^{CTD}, *Pa*^{Nter}-*Pp*^{CTD}) without arabinose and with *P. entomophila* L48 wild-type, L48 Δ*exlBA* expressing *exlBA*^{Pe} (*Pe*), *exlBA*$^{Pe-Nter}$ (*Pe*^{Nter}) and the chimeric proteins (*Pe*^{Ner}-*Pa*^{CTD}, *Pe*^{Nter}-*Pp*^{CTD}) in presence of 0.01% of arabinose. For each bacterium, a superposed image of transmission and PI-fluorescence is shown, with zoom at several selected cells. Scale bar represents 50 μm. Cells were lysed after the infection and proteins recovered in the lysate were separated on a gradient of 4-20% acrylamide Tris-glycine gel and analyzed by Western blotting using anti-E-cadherin antibodies. Anti-β-actin antibodies were used as a loading control to normalize E-cadherin bands. 100% correspond to the non-infected condition. CTD of *Pa* increases ExlA^{Pe} cytotoxic activity but does not provoke the E-cadherin cleavage during *P. entomophila* infection, whereas ExlA^{Pa} chimeras with CTD of *P. entomophila* and *P. putida* partially restores the ExlA^{Pa} activity. The experiment for cadherin quantification was repeated three times; one representative western blot and quantification are shown.

at the CTD is important for the cytotoxicity and can be exchanged between the two CTD classes. Similar to ExlA^{Pa}, the absence of CTD in the *P. entomophila* protein (ExlA$^{Pe-Nter}$) resulted in a reduced cytotoxicity. Chimeric proteins are significantly different from full-length ExlA^{Pe}, with ExlA$^{PeNter\text{-}PaCTD}$ being more active and ExlA$^{PeNter\text{-}PpCTD}$ less active than the native protein; however, they were both significantly more cytotoxic than ExlA$^{Pe-Nter}$.

As the E-cadherin integrity can serve as a read-out of the pore-forming activity of ExlA through ADAM10 activation, we tested its cleavage by immunoblot and imaged the infection process by microscopy. None of the chimeric proteins in *P. entomophila* induced the cleavage of E-cadherin, nor cell-to-cell adhesion rupture or cell rounding during infection (Figure 4C), although they all caused PI incorporation. This result shows notably, that the CTD of ExlA^{Pa} is not sufficient to form a pore in association with ExlA$^{Pe-Nter}$. On the contrary, in *P. aeruginosa* the ExlA$^{Pa-Nter}$ chimeric proteins with CTD of *P. entomophila* or *P. putida* induced partial cleavage of E-cadherin with the partial loss of cell-to-cell adhesion (Figure 4C), showing that the presence of any CTD could partially restore the ExlA^{Pa} pore-forming activity. Together, these results suggest that these ExlA orthologues may induce cell death through different mechanisms and that the CTDs and N-terminal domains with FHA repeat domains define together the protein function.

ExlA-like proteins contribute to virulence in *Galleria mellonella* larvae and *Drosophila* flies

We then sought to determine the role and the activity of ExlA proteins *in vivo*, in known hosts or targets such as fungi, amoeba, and insect larvae for *P. chlororaphis* (Kupferschmied et al., 2013; Pukatzki et al., 2002) and *Drosophila* flies for *P. entomophila* (Opota et al., 2011; Vallet-Gely et al., 2010b). We first tested the capacity of *P. chlororaphis* to inhibit the growth of the fungal plant pathogens *Sclerotinia sclerotiorum* and *Botrytis cinerea* (Manuel et al., 2012; Savchuk and Dilantha Fernando, 2004), using radial inhibition assays on agar plates. No significant difference in growth inhibition of these two fungi was observed, showing that the ExlA toxin does not participate in the fungicide activity of PA23 (Figure S7A). We then wondered if ExlA could influence the growth of eukaryotic organisms such as amoeba. To test whether *P. chlororaphis* could infect *Acanthamoeba castellani*, the cytotoxicity of *P. chlororaphis* cells was determined by using a simple plating assay (Pukatzki et al., 2002). No difference in plaque formation was observed between wild-type and Δ*exlBA* strains (Figure S7B).

P. chlororaphis strains possess oral and systemic insecticidal activity (Flury et al., 2016) and *P. entomophila* is a natural entomopathogen (Vodovar et al., 2006). To assess whether there is a contribution of ExlA toxins to insect killing, we used *G. mellonella* larvae and *Drosophila melanogaster* adult flies, as models. As we previously reported (Trouillon et al., 2020), the wild-type strain PA23 efficiently kills *G. mellonella* larvae, whereas the Δ*exlBA* mutant was significantly attenuated (Figure 5A inset). When other *P. chlororaphis* strains were injected into the hemocoel of the larvae (approx. 6×10^4 CFU), mortality occurred within 18-26 h post-injection with typical changes in color of the larvae due to melanization, an immune response of the larvae (Figures 5A, S8A, and S8B). The *P. chlororaphis* strain CIP75.23 was more virulent than the CIP63.22T strain, in accordance with *in vitro* results on cytotoxicity and the higher amounts of secreted ExlA (Figures 5A and S8), further suggesting a contribution of ExlA^{Pch} to larvae mortality. We then tested the ability of *P. entomophila* strains to kill *G. mellonella* using similar conditions as those established for *P. chlororaphis* (approx. 6×10^4 CFU, incubation at 30°C). Both Δ*mnl* and Δ*gacA* mutants displayed attenuated *Galleria* killing compared to the parental strain, confirming the role of the pore-forming Monalysin in this infection model. In both genetic backgrounds, the inactivation of *exlA* resulted in significantly less virulent strains (Figure 5A) with additive effects, confirming that the ExlA protein of *P. entomophila* plays a role, although probably different than Monalysin and other GacS/GacA regulated genes, in establishing a pathogenic relationship with the host.

As *P. entomophila* was originally isolated from dead flies and is a natural pathogen for *D. melanogaster* (Vodovar et al., 2005), we tested if ExlA contributes to *D. melanogaster* killing by feeding or pricking. As previously reported (Opota et al., 2011; Vallet-Gely et al., 2010a), female flies fed with high doses of *P. entomophila* died within 2-4 days, while in the same experimental conditions, *P. chlororaphis* PA23 provoked low fly mortality over several days, independently of the presence of ExlA (Figure S8C). Surprisingly, although single mutants of Monalysin and GacA were less virulent than the wild-type *P. entomophila* strain (Opota et al., 2011), inactivation of the *exlBA* operon in these three genetic backgrounds had no impact on bacteria-induced fly killing (Figure S8C, lower panel). Recent work by Vesga et al. showed that the *PPRCHA0_4278* gene encoding the TpsA/ExlA in *P. protegens* was induced when bacteria are injected

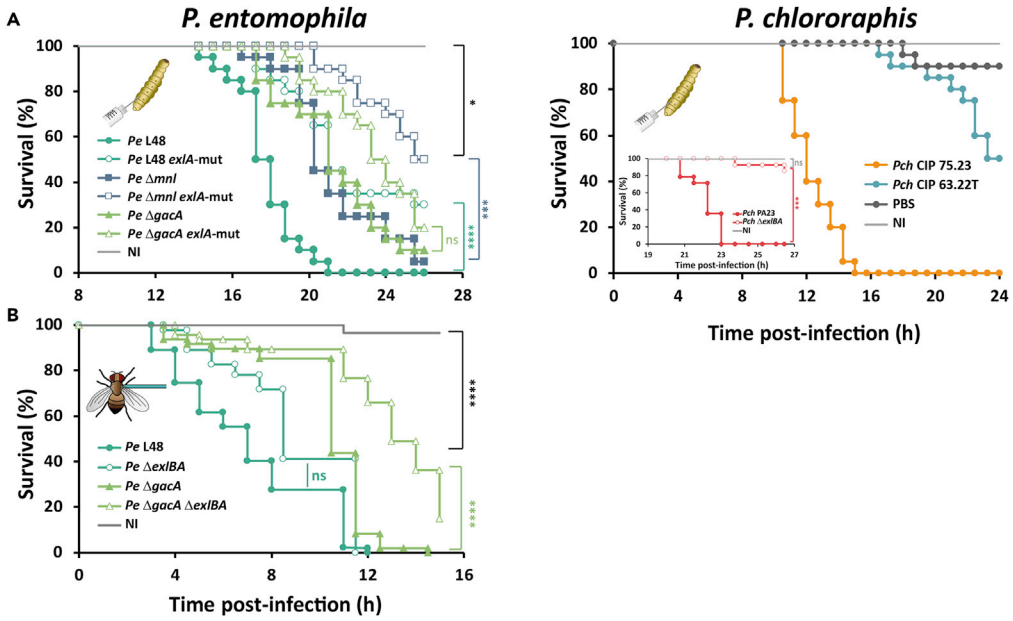

Figure 5. ExlA contributes to killing of fruit fly *Drosophila melanogaster* and larvae of wax moth *Galleria mellonella*

(A) Survival of *G. mellonella* larvae (N = 20) after injection of *P. entomophila* L48 strain (*Pe*) (left panel) wild type (green cyan), Δ*mnl* (deep blue), Δ*gacA* (light green), and the respective *exlA*-mut in open symbols. Infection with different strains of *P. chlororaphis* (*Pch*) (right panel), reference strain PA23 wild-type and Δ*exlBA* are shown in inset panel. Other strains of *Pch* are presented in Figure S8. Survival rates of the larvae are expressed as percentage (%). Larvae were injected with approx. 6 × 10^4 bacteria in PBS, and let at 30°C. Control larvae were injected with sterile PBS.

(B) *Drosophila melanogaster* infection (N = 50) with indicated *P. entomophila* strain. *Pe* were injected into the thorax of female *Drosophila* flies using a needle dipped into a bacterial suspension. The fly survival was monitored at room temperature. *P. entomophila* L48 (filled circle), the single mutant Δ*exlA* (open circle), Δ*gacA* (filled triangle), and the double mutant Δ*gacA*Δ*exlA* (open triangle) were resuspended in sterile PBS corresponding to OD_{600} of 20. For all experiments, Log-rank test was used to determine statistically significant difference with $p \leq 0.05$ (*), $p \leq 0.01$ (**), $p \leq 0.001$ (***), $p \leq 0.0001$ (****), ns: not significant. Pricking experiment was repeated five times. See also Figures S7 and S8.

into the larvae hemocoel, in which the protein might have a specific role in evading the insect immune system (Vesga et al., 2020). This prompted us to inject bacteria directly into the hemocoel of the fly and to evaluate its contribution to virulence. Indeed, the contribution of ExlA was observed when using the Δ*gacA* genetic background, in which the deletion of the *exlBA* operon resulted in significantly delayed fly killing (Figure 5B). Together, our results showed that, in two different *Pseudomonas* species, the disruption of a gene encoding the TPS toxin ExlA reduced bacterial toxicity toward different insects revealing the role of this TPS in pathogenic bacteria-insect interactions.

Comparative genomics of the regions containing *exlA* and *exlB* genes in different *Pseudomonas* species suggests different evolutionary histories

To better understand the evolution of the *exlBA* operon in the different *Pseudomonas* species, we examined their genomic context across pathogenic and environmental isolates of *Pseudomonas* (Figure 6 and Table S4). This revealed that, although $ExlB^{Pch}$ and $ExlA^{Pch}$ are highly similar in sequence to the proteins of *P. aeruginosa*, the genomic environment of the operon is different compared to *P. aeruginosa* but conserved when compared to *P. protegens* (Figure 6). Furthermore, the analyses of three *P. putida* strains (reference strain KT2440 and strains S13 and E41) showed that genomic synteny is conserved only on one side of the *exlBA* cluster (Figure 6). Indeed, strain *P. putida* KT2440 is part of a small group of strains with conserved synteny, but synteny breaks are present compared to the rest of the *P. putida* strains analyzed (Figure S9). This clearly suggests that a genomic rearrangement took place in the ancestor of the small group that contains among others the *P. putida* KT2440 strain. In contrast, genomic synteny is completely lost when analyzing *P. entomophila* 2014 and the widely used L48 strain (Figure 6).

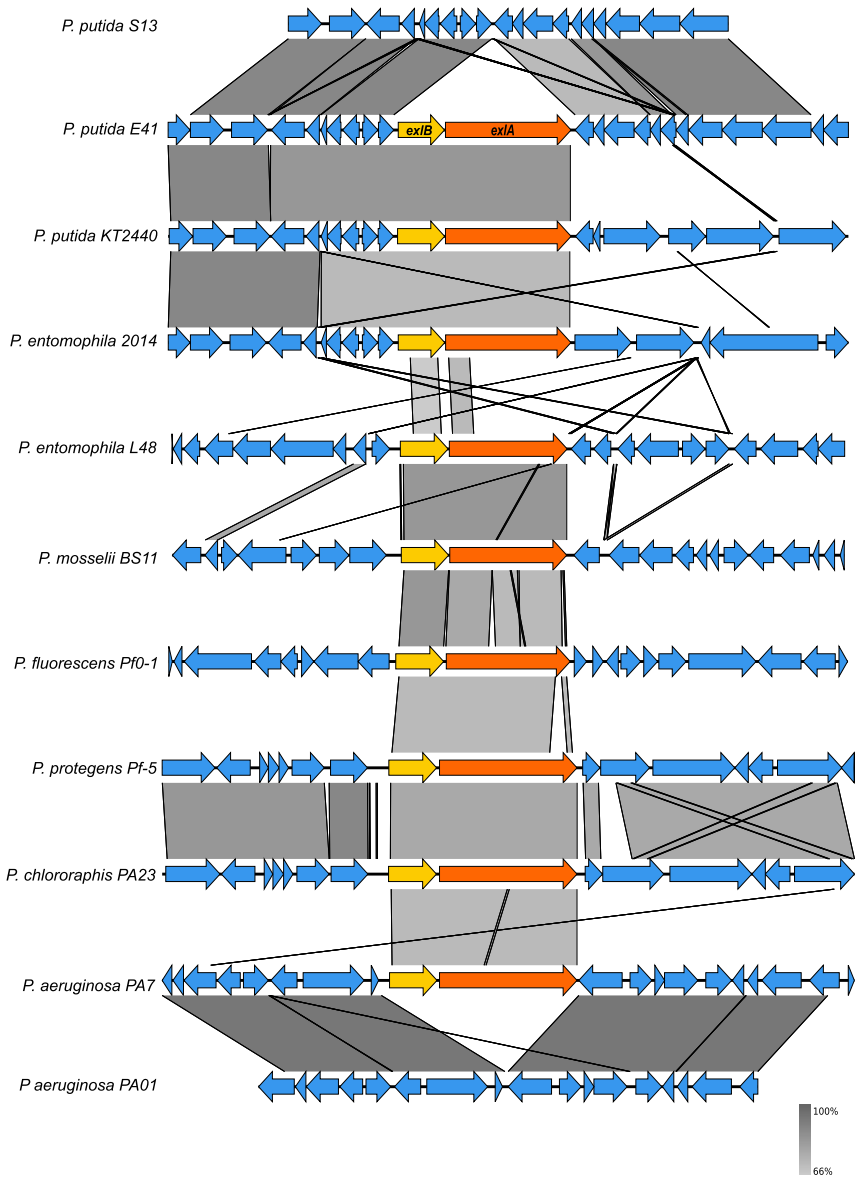

Figure 6. Graphical representation of the genomic context and BLASTn comparison of the region containing the *exlBA* locus in selected *Pseudomonas* strains

Protein-coding regions are represented by arrows (yellow and orange arrows represent *exlB* and *exlA* genes, respectively). The gradient gray shading represents regions of nucleotide sequence identity (100%–66%) determined by BLASTn analysis. Figures are drawn to scale using Easyfig 2.2.2 (Sullivan et al., 2011). See also Figure S9.

This first genomic comparison pointed to a complex history of the evolution of the *exlBA* operon in the genus *Pseudomonas*. Thus, to better understand the evolution of the operon in the analyzed *Pseudomonas* strains, we constructed phylogenetic trees of both ExlA/B proteins as well as a *Pseudomonas* species tree, which allowed us to compare the species versus gene histories.

The evolutionary history of the *exlBA* operon in the genus *Pseudomonas* is complex

To analyze the evolution of the *Pseudomonas* species/strains containing *exlBA* used in this study, we constructed a phylogeny based on their core set of genes using *Burkholderia cepacia* strains as outgroup (Figures 7 and S13). The phylogenetic tree we obtained is congruent with phylogenetic studies of the *Pseudomonas* genus published previously (Gomila et al., 2015; Garrido-Sanz et al., 2016; Peix et al., 2018;

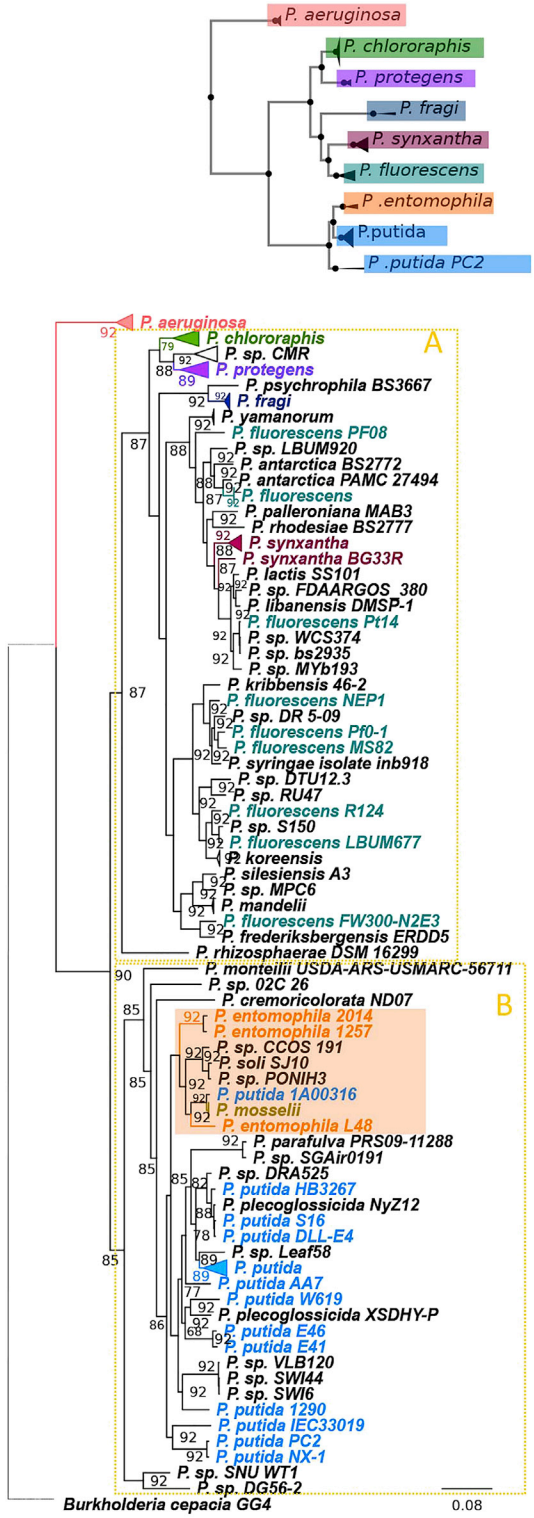

Species tree

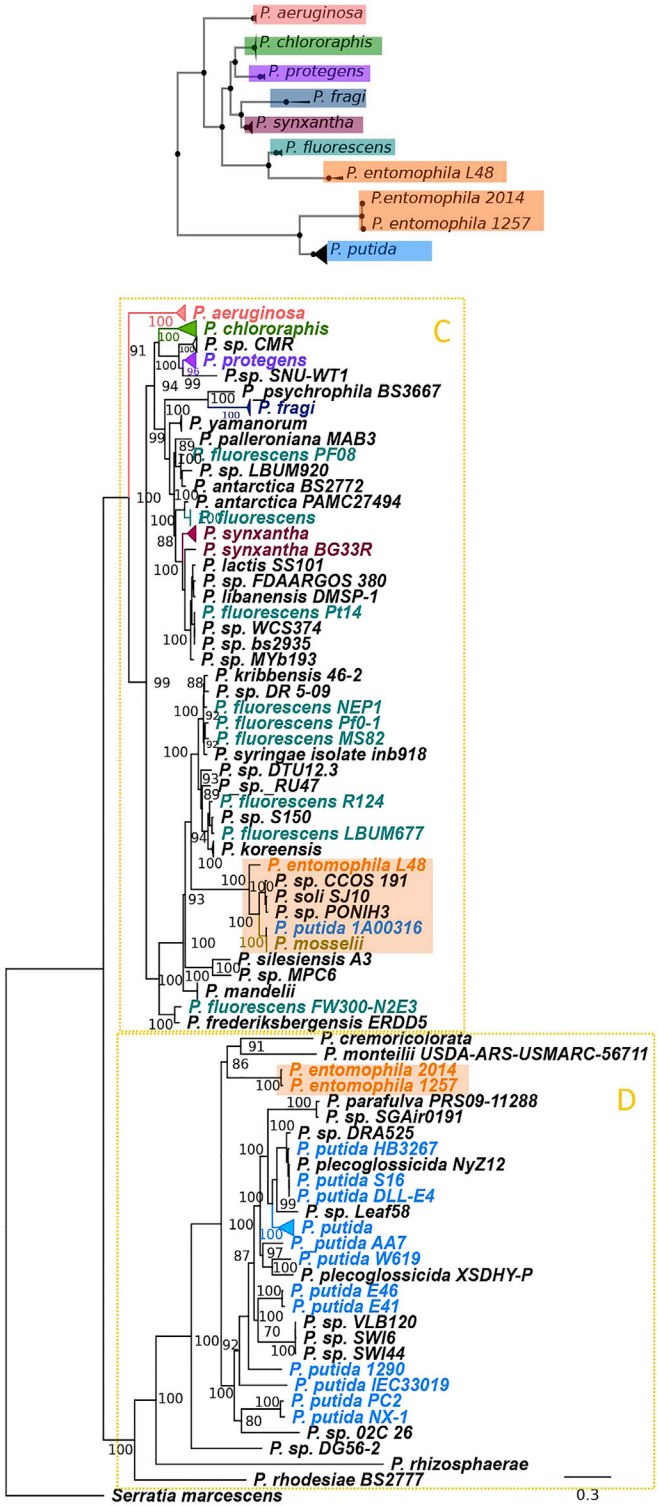

ExIA Tree

Figure 7. *Pseudomonas* species tree versus ExlA tree

In the upper right side of each tree, a small-condensed version is represented to clearly visualize the main clades. The main clusters of each phylogeny (A, B, C, and D) are highlighted by a yellow square. Orange squares highlight the main *P. entomophila* clusters in each tree. Numbers beside each node represent node support values: Gene support indices (GSIs) for the species tree and percentage bootstrap values after 1000 bootstrap replicates for the ExlA tree. Scale bar on the bottom of each tree indicates the estimated number of amino acid substitutions per site. Both trees are rooted using outgroup species: *Burkholderia cepacia* strains in the case of the *Pseudomonas* species tree and *Serratia marcescens* for the ExlA tree. The branch leading to *B. cepacia* is represented by a dotted line in the species tree, has been shortened to adapt the size of the figure, and does not represent the real distance. See also Figures S2, S10–S13, and Table S6.

Lalucat et al., 2020). The *Pseudomonas* species containing the *exlBA* operon are distributed in two main clades: one containing among others *P. chlororaphis*, *P. protegens*, and *P. fluorescens* strains (Figure 7, clade A), and a second one containing mostly *P. putida* and *P. entomophila* strains (Figure 7, clade B), whereas *P. aeruginosa* strains localize outside these two main clusters. When we reconstruct the same tree but include also *Pseudomonas* strains that do not contain the *exlBA* operon like done previously (Trouillon et al., 2020) (Figure S13), the patchy distribution of strains containing *exlBA* suggests that these genes were acquired through HGT.

To gain insight into the evolutionary history of this locus in the genus *Pseudomonas*, we performed phylogenetic tree reconstruction of both proteins, ExlA and ExlB, using maximum likelihood and Bayesian inference. The trees obtained with the different reconstruction methods were similar for both proteins, indicating that a strong phylogenetic signal is present on both sequences (Figures S10 and S11). Moreover, the trees obtained from ExlA and ExlB were also highly congruent (Figure S12), which suggests that both genes have been transferred together within the genus *Pseudomonas*, in agreement with their strong co-occurrence in different *Pseudomonas* species and their functional relationship. However, the comparison of the *Pseudomonas* species tree and the ExlA/ExlB phylogenies reveals many topological differences between both trees (Figure 7), which suggests that HGT of these two genes between *Pseudomonas* species/strains has also occurred. One of these main differences is the distribution of *Pseudomonas* species in two main groups in the ExlA/B trees (clusters C and D, Figure 7) that do not correspond exactly to the two main groups in the species tree (clusters A and B in Figure 7) in which one contains mainly *P. putida* and some *P. entomophila* strains and the other one mainly *P. aeruginosa*, *P. chlororaphis*, *P. protegens*, and *P. fluorescens*. Based on this analysis, the ExlA/B proteins encoded by *P. aeruginosa* are closer to those of *P. chlororaphis* or *P. protegens* than to those of *P. putida*. This result is supported by both ExlA and ExlB phylogenies with high support values, and it is also congruent with our previous sequence analyses showing a higher amino acid identity between ExlA/B from *P. aeruginosa* and *P. chlororaphis* than with that of the *P. putida* cluster. This suggests HGT of these genes between the ancestor of *P. aeruginosa* strains containing the locus and *Pseudomonas* species of cluster A of the phylogeny (Figure 7).

Another main difference is the phylogenetic position of *P. entomophila* strains in the ExlA/B tree, in which the group of *P. entomophila* L48 and *P. mosselii* does not cluster with *P. putida* strains but with the *P. fluorescens* group. In contrast, the other two *P. entomophila* strains (2014/1257) analyzed here cluster with *P. putida* strains like in the phylogeny of the genus (Figure 7). This result is also in agreement with our previous observation of a higher amino acid identity and synteny between *P. putida* and *P. entomophila* 2014/1257 strains in comparison to *P. entomophila* L48 and explains the differences we observed between strain L48 and *P. entomophila* strains 2014/1257 in sequence identity and synteny.

The *exlBA* operon has been acquired several times during the evolution of the genus *Pseudomonas*

The analyses of the genomic context of the *exlBA* operon in the different *Pseudomonas* species revealed that, upstream of *exlB*, the synteny is conserved in all species belonging to the clade B of the *Pseudomonas* phylogeny (Figures 6 and 7), as the *exlBA* genes are situated always downstream the *ytgC* gene. However, the strains belonging to the smallest cluster that contains *P. entomophila* L48 and *Pseudomonas* sp. CCOS191 (orange square, Figure 8) is an exception. In these species, the *exlBA* genes localize in a different genomic region. This is in agreement with the acquisition of the *exlBA* genes by HGT in the ancestor of these strains, as predicted by our previous results. However, the observation that, in all other species belonging to clade B, *exlBA* are downstream the *ytgC* gene suggests that the most parsimonious scenario is that the *exlBA* cluster was also present in this region in the ancestor of the clade *P. entomophila* L48 and *Pseudomonas* sp. CCOS191, and it might have been lost later. To test this hypothesis, we analyzed the

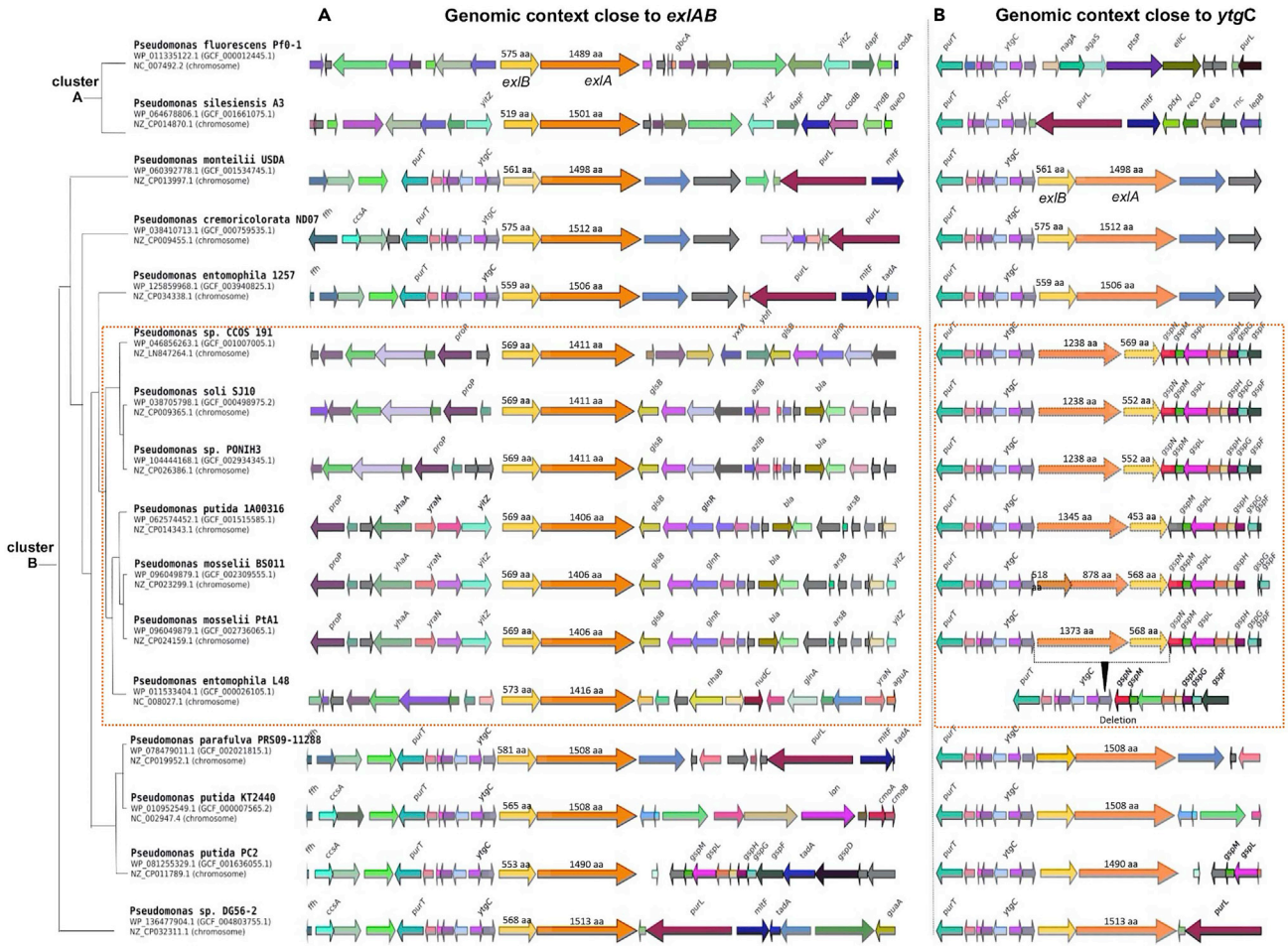

Figure 8. Comparison of the genomic regions containing *exlBA* of *Pseudomonas* species belonging to the cluster *L. entomophila* L48/P. sp. CCOS191 with selected species phylogenetically related to this cluster

(A) *exlBA* operon and its genomic environment in selected species.

(B) Genomic region containing the *ytgC* gene, the genomic location of *exlBA* or *exlAB* operon in the species belonging to cluster B of *Pseudomonas*. Synteny has been analyzed with the software GeneSpy (Garcia et al., 2019). Orange square indicates the cluster *L. entomophila* L48/P. sp. CCOS191. See also Figure S2.

genomic context around the *ytgC* gene in the species of the *P. entomophila* L48 and *Pseudomonas* sp. CCOS191 cluster. Most interestingly, except for strain *P. entomophila* L48, all strains belonging to this cluster contained in this genomic location also sequences with partial homology to *exlB* and *exlA* genes (Figure 8). However, these *exlBA* homologous genes were shorter compared to the genuine *exlBA* genes in the same strains, and even fragmented in some strains (e.g., homologous of *exlA* in strain *P. mosselii* PtA1). Secondly, in these strains, the order of the genes is inverted with respect to the genuine *exlBA* cluster. Thirdly, these homologs had a higher identity with other *exlBA* homologs or genes located downstream of *ytgC* in other strains of the clade B than to the genuine *exlBA* genes from the same strain. This clearly indicates a different origin for the two *exlBA* operons and their homologs close to *ytgC*. Indeed, the analyses of all results suggest, as the most parsimonious scenario of evolution of these genes, that although originally the *exlBA* operon was in the same gene location for all strains belonging to clade B, these genes were duplicated in the species belonging to the small cluster containing *P. entomophila* L48 and *Pseudomonas* sp. CCOS191 due to the acquisition of a second *exlBA* cluster through an HGT event resulting in *exlBA* xenologs. The presence of duplicated copies in these strains, the original orthologs of *exlBA* and the acquired xenologs, probably led to a pseudogenization process of the original ortholog *exlBA* operon that is still ongoing, except in strain L48 in which the original *exlBA* cluster has been completely removed.

DISCUSSION

In this work, we characterized several ExlB-ExlA TPSs encoded in genomes of environmental *Pseudomonas* species that are non-pathogenic for humans. Originally annotated in the databases as secreted filamentous hemagglutinins, adhesins or hemolysins, most of the *Pseudomonas* ExlA proteins share similar size (150-170 kDa), conserved TPS domains and have a central part encoding FHA domains. Based on the primary sequences of the TPS domain and their smaller size, they can be phylogenetically separated from the TPS adhesins, proteins with contact-dependent inhibition activity (CDIs) and other TPS proteins with iron-acquisition activities (Guerin et al., 2017; Mazar and Cotter, 2007). Indeed, the *P. aeruginosa* ExlA groups with the well-studied hemolysins ShlA from *Serratia marcescens* and PhlA from *Photorhabdus luminescens*. Here we show that the family of *Pseudomonas* ExlA proteins can be further sub-classified into two groups depending on their CTDs and activity toward host-cell membranes. ExlA proteins of *P. aeruginosa* and *P. chlororaphis* incorporate within lipid rafts of epithelial membranes, which results in the cleavage of the cell-cell junction protein E-cadherin. The cleavage occurs as a consequence of ExlA-dependent pore formation, massive influx of Ca^{2+} which activates in turn the host protease ADAM10 (Reboud et al., 2017). E-cadherins are natural substrates of the ADAM10 metalloprotease and frequent targets of bacterial pathogens through a variety of mechanisms (Huber, 2020). ExlA proteins of *P. entomophila* and *P. putida* although being associated with epithelial membranes did not provoke any cleavage of the E-cadherin protein, suggesting that the ExlA-dependent mechanisms leading to epithelial cell dysfunction or death differ between the species analyzed here. There are many examples where polymorphic toxins, including CDIs from the TPS family, carry functions in CTDs (Ruhe et al., 2020; Zhang et al., 2012). We showed previously that the pore-forming activity of $ExlA^{Pa}$ is contained in its disordered, molten globule CTD (Basso et al., 2017; Bertrand et al., 2020). Indeed, the CTDs of *P. chlororaphis* and *P. aeruginosa* are 64% identical and show the same functional activity, e.g., pore-formation, cell rounding during infection, cleavage of E-cadherin, and both proteins incorporate into lipid rafts. In contrast, ExlA orthologs from *P. entomophila* and *P. putida* have shorter CTDs, and their interaction with the host membranes is different, e.g., there is no cleavage of E-cadherin and consequently no cell rounding, clearly suggesting different modes of action. Small differences in amino acid sequences, notably divergent CTDs, may alter the capacity of proteins to form pores within host membranes, probably through a different fold of molten globules. However, there is a clear contribution of FHA domains in pore-forming activity of the protein, as the chimera between the N-terminal of $ExlA^{Pe}$ carrying CTD of $ExlA^{Pa}$ did not restore E-cadherin cleavage.

The *P. chlororaphis* and *P. entomophila* ExlA proteins contributed to toxicity in *G. mellonella* larvae. This finding might open the possibility to modulate ExlA levels and to increase the use of these *Pseudomonas* species in management of pest insects (Keel, 2016; Kupferschmied et al., 2013). Some entomopathogens, such as *Photorhabdus* and *Xenorhabdus* strains, are currently used as bio-insecticides in agriculture thanks to the activity based on the tripartite toxin complex (Tc) production (Liu et al., 2010) composed of TcdA/TcdB/TccC (Yang and Waterfield, 2013). The *P. entomophila* strain analyzed here also possesses the genes encoding TccC-type toxin and proteomic analysis identified the protein. Possible interactions or cooperation of the Tcc toxin with ExlA in insect killing will be investigated further. Moreover, some entomopathogens use the type VI secretion machinery (T6SS) to target insect microbiota (Vacheron et al., 2019). Cooperation between TPS substrates and toxins exported by different secretion machineries should be considered as virulence of entomopathogens is multi-factorial (Keel, 2016). We can speculate that ExlA proteins somehow contribute to the modulation of the host immune response by acting on macrophages, as recently proposed for ExlA from *P. protegens* (Vesga et al., 2020, 2021). In *P. aeruginosa*, two regulatory elements dictate *exlBA* expression: the activating Vfr/cAMP pathway and the Cro/CI-like repressor ErfA (Berry et al., 2018; Trouillon et al., 2020). Interestingly, none of the *exlB* promoters in different *Pseudomonas* display conserved Vfr DNA-binding sites and ErfA regulation was found to be *P. aeruginosa*-specific (Trouillon et al., 2020), suggesting novel, species-specific regulatory pathways governing the activation of the *exlBA* operons. The regulatory mechanisms governing expression of *exlBA* TPS operons in different species need to be investigated in the future, as the spatiotemporal expression of virulence factors may be essential for invasion of insect hosts by bacterial pathogens. Furthermore, the molecular tools developed in this work may allow the investigation of the mechanistic features of ExlA directly in their natural hosts.

It is intriguing, that even if only some *Pseudomonas* species contain the ExlA/B proteins, they have evolved different functions. Indeed, our evolutionary analyses demonstrate that the *exlBA* operon has moved horizontally within the genus *Pseudomonas*, explaining why the similarity values between *exlBA* from different species are not always congruent with the phylogenetic distance between them. We identified a first

putative HGT event suggesting that the *exlBA* operon might have jumped between the ancestor of some *P. aeruginosa* strains and some species of the cluster *P. fluorescens/P. chlororaphis*, although the direction of the transfer cannot be established based on our results. A second transfer event has been identified in the cluster of *P. entomophila* L48 and *Pseudomonas* sp. CCOS191, shedding light on the particularities of *exlBA* from *P. entomophila* L48 strain compared to other *P. entomophila* strains. The phylogenetic results predicted that the transfer occurred from one species of the cluster *P. fluorescens/P. mandelii* to the ancestor of the *P. entomophila* L48/*Pseudomonas* sp. CCOS191 group. Interestingly, the analysis of the genomic context of the *exlBA* in these species led us to reconstruct the evolutionary history of the *exlAB* operon in this cluster. Indeed, our results suggest that the acquisition of a second *exl* operon in the ancestor of this group gave place to the disintegration of the ancestral *exlBA* genes through a gene erosion process that is still ongoing.

Horizontal movement of the *exlBA* operon is probably also responsible for the emergence of these TPSs in the genus *Pseudomonas*, as suggested from the patchy distribution of *exlBA* genes on the *Pseudomonas* phylogeny. The determination of the putative source of acquisition of this operon by different *Pseudomonas* species is out of the scope of this study. However, a homologous search by blast revealed a surprisingly high sequence similarity of *Pseudomonas* ExlA with proteins from nematodes (46% identity and 87% coverage with a hypothetical protein of the nematode species *Dyploscapter pachys*). Given that nematodes have been described as natural hosts of *Pseudomonas*, HGT between them is highly likely and should be explored in the future. The acquisition of genes from a eukaryotic host, as it has been shown for *Legionella pneumophila* (Gomez-Valero and Buchrieser, 2019), is an efficient way to integrate new functions, and increasing adaptability in these organisms could also be possible for *Pseudomonas*.

Taken together, our analyses shed light on the dynamics of the *exlBA* operon within the genus *Pseudomonas* and demonstrated that HGT and genomic erosion shaped functional differences in the *exlBA* operon from different species that might have been acquired from a nematode host.

Limitations of the study

In this study, we functionally characterized ExlA-like toxins in restricted and representative strains of non-*P. aeruginosa*. Phylogenetic studies showed that strains differ greatly in the *exlBA* sequences and their genetic environment. More comprehensive functional approach could be applied to other strains to apprehend global diversity of ExlA functions.

STAR★METHODS

Detailed methods are provided in the online version of this paper and include the following:

- KEY RESOURCES TABLE
- RESOURCE AVAILABILITY
  - Lead contact
  - Materials availability
  - Data and code availability
- EXPERIMENTAL MODEL AND SUBJECT DETAILS
  - Bacterial strains and culture cell conditions
  - *Drosophila* and *Galleria*
- METHOD DETAILS
  - Genetic constructions
  - Cytotoxicity assays and microscopy
  - E-cadherin cleavage
  - Lipid raft isolation and western blotting
  - Cytoplasmic membranes purifications
  - Amoeba growth by plaque formation assay
  - *Galleria mellonella* infection
  - *Drosophila* infections
  - Evolutionary analyses
- QUANTIFICATION AND STATISTICAL ANALYSIS
  - Statistics
  - Mass spectrometry-based quantitative proteomic analysis of secretomes

SUPPLEMENTAL INFORMATION

Supplemental information can be found online at https://doi.org/10.1016/j.isci.2022.104596.

ACKNOWLEDGMENTS

We thank Isabelle Vallet-Gely and Bruno Lemaitre for providing the *P. entomophila* mutants and plasmids, and Teresa de Kievit for *P. chlororaphis* PA23 strain. *P. aeruginosa* IHMA87 was obtained from the International Health Management Association, USA. We would like to thank Emma Chastaing for her technical assistance for the experiments with amoebae and fungi during her master internship (MAP, Lyon). We thank Emmanuel Tailleboug for the technical assistance in *Drosophila melanogaster* experiments. The work was supported by grants from Agence Nationale de la Recherche (ANR-15-CE11-0018-01), the Laboratory of Excellence GRAL, financed within the University Grenoble Alpes graduate school (Ecoles Universitaires de Recherche) CBH-EUR-GS (ANR-17-EURE-0003) and the Fondation pour la Recherche Médicale (Team FRM 2017; DEQ20170336705) to I.A. We acknowledge the receipt of different *Pseudomonas* strains from the Collection of the Institut Pasteur (CIP). Work in the CB laboratory is financed by the Institut Pasteur and the grant n ANR-10-LABX-62-IBEID. Proteomic experiments were partially supported by ProFI (Proteomics French Infrastructure, ANR-10-INBS-08).

AUTHOR CONTRIBUTIONS

I.A., C.B., and V.J. designed the study; V.J., A.R., S.B., M.R.G., P.P., E.G., and S.E. performed the experiments and analyzed the data; L.G.V., C.R., and V.C.F. performed the genomic analysis; A.A. and Y.C. performed and analyzed MS/proteomic data; K.J. and M.O.F. provided tools and materials; C.B. and I.A. wrote the manuscript; and all authors edited the manuscript.

DECLARATION OF INTERESTS

The authors declare no competing interests.

Received: November 17, 2021
Revised: March 15, 2022
Accepted: June 8, 2022
Published: July 15, 2022

SUPPORTING CITATIONS

The following reference appears in the Supplemental Information: Robinson et al., 2016.

REFERENCES

Basso, P., Ragno, M., Elsen, S., Reboud, E., Golovkine, G., Bouillot, S., Huber, P., Lory, S., Faudry, E., and Attree, I. (2017). Pseudomonas aeruginosa pore-forming exolysin and type IV pili cooperate to induce host cell lysis. mBio *8*, e02250-16. https://doi.org/10.1128/mBio.02250-16.

Baud, C., Hodak, H., Willery, E., Drobecq, H., Locht, C., Jamin, M., and Jacob-Dubuisson, F. (2009). Role of DegP for two-partner secretion in bordetella. Mol. Microbiol. *74*, 315–329. https://doi.org/10.1111/j.1365-2958.2009.06860.x.

Baynham, P.J., Ramsey, D.M., Gvozdyev, B.V., Cordonnier, E.M., and Wozniak, D.J. (2006). The Pseudomonas aeruginosa ribbon-helix-helix DNA-binding protein AlgZ (AmrZ) controls twitching motility and biogenesis of type IV pili. J. Bacteriol. *188*, 132–140. https://doi.org/10.1128/JB.188.1.132-140.2006.

Berry, A., Han, K., Trouillon, J., Robert-Genthon, M., Ragno, M., Lory, S., Attrée, I., and Elsen, S. (2018). cAMP and Vfr control exolysin expression and cytotoxicity of Pseudomonas aeruginosa taxonomic outliers. J. Bacteriol. *200*, e00135-18. https://doi.org/10.1128/jb.00135-18.

Bertrand, Q., Job, V., Maillard, A.P., Imbert, L., Teulon, J.M., Favier, A., Pellequer, J.L., Huber, P., Attrée, I., and Dessen, A. (2020). Exolysin (ExlA) from Pseudomonas aeruginosa punctures holes into target membranes using a molten globule domain. J. Mol. Biol. *432*, 4466–4480. https://doi.org/10.1016/j.jmb.2020.05.025.

Bouillot, S., Pont, S., Gallet, B., Moriscot, C., Deruelle, V., Attrée, I., and Huber, P. (2020). Inflammasome activation by Pseudomonas aeruginosa's ExlA pore-forming toxin is detrimental for the host. Cell Microbiol. *22*, e13251. https://doi.org/10.1111/cmi.13251.

Bouyssié, D., Hesse, A.M., Mouton-Barbosa, E., Rompais, M., Macron, C., Carapito, C., Gonzalez de Peredo, A., Couté, Y., Dupierris, V., Burel, A., et al. (2020). Proline: an efficient and user-friendly software suite for large-scale proteomics. Bioinformatics *36*, 3148–3155. https://doi.org/10.1093/bioinformatics/btaa118.

Casabona, M.G., Vandenbrouck, Y., Attree, I., and Couté, Y. (2013). Proteomic characterization of Pseudomonas aeruginosa PAO1 inner membrane. Proteomics *13*, 2419–2423. https://doi.org/10.1002/pmic.201200565.

Clantin, B., Hodak, H., Willery, E., Locht, C., Jacob-Dubuisson, F., and Villeret, V. (2004). The crystal structure of filamentous hemagglutinin secretion domain and its implications for the two-partner secretion pathway. Proc. Natl. Acad. Sci. USA *101*, 6194–6199. https://doi.org/10.1073/pnas.0400291101.

Darriba, D., Taboada, G.L., Doallo, R., and Posada, D. (2011). ProtTest 3: fast selection of best-fit models of protein evolution. Bioinformatics *27*, 1164–1165. https://doi.org/10.1093/bioinformatics/btr088.

Delattre, A.-S., Saint, N., Clantin, B., Willery, E., Lippens, G., Locht, C., Villeret, V., and Jacob-Dubuisson, F. (2011). Substrate recognition by the POTRA domains of TpsB transporter FhaC. Mol. Microbiol. *81*, 99–112. https://doi.org/10.1111/j.1365-2958.2011.07680.x.

Do, C.B., Mahabhashyam, M.S.P., Brudno, M., and Batzoglou, S. (2005). ProbCons: probabilistic consistency-based multiple sequence alignment. Genome Res. *15*, 330–340. https://doi.org/10.1101/gr.2821705.

Elsen, S., Huber, P., Bouillot, S., Couté, Y., Fournier, P., Dubois, Y., Timsit, J.F., Maurin, M., and Attrée, I. (2014). A type III secretion negative clinical strain of Pseudomonas aeruginosa employs a two-partner secreted exolysin to induce hemorrhagic pneumonia. Cell Host Microbe *15*, 164–176. https://doi.org/10.1016/j.chom.2014.01.003.

Faccone, D., Pasteran, F., Albornoz, E., Gonzalez, L., Veliz, O., Prieto, M., Bucciarelli, R., Callejo, R., and Corso, A. (2014). Human infections due to Pseudomonas chlororaphis and Pseudomonas oleovorans harboring new bla(VIM-2)-borne integrons. Infect. Genet. Evol. *28*, 276–277. https://doi.org/10.1016/j.meegid.2014.10.012.

Faudry, E., Job, V., Dessen, A., Attree, I., and Forge, V. (2007). Type III secretion system translocator has a molten globule conformation both in its free and chaperone-bound forms. FEBS J. *274*, 3601–3610. https://doi.org/10.1111/j.1742-4658.2007.05893.x.

Fauvarque, M.O., Bergeret, E., Chabert, J., Dacheux, D., Satre, M., and Attree, I. (2002). Role and activation of type III secretion system genes in Pseudomonas aeruginosa-induced Drosophila killing. Microb. Pathogen. *32*, 287–295. https://doi.org/10.1006/mpat.2002.0504.

Flury, P., Aellen, N., Ruffner, B., Péchy-Tarr, M., Fataar, S., Metla, Z., Dominguez-Ferreras, A., Bloemberg, G., Frey, J., Goesmann, A., et al. (2016). Insect pathogenicity in plant-beneficial pseudomonads: phylogenetic distribution and comparative genomics. ISME J. *10*, 2527–2542. https://doi.org/10.1038/ismej.2016.5.

Garcia, P.S., Jauffrit, F., Grangeasse, C., and Brochier-Armanet, C. (2019). GeneSpy, a user-friendly and flexible genomic context visualizer. Bioinformatics *35*, 329–331. https://doi.org/10.1093/bioinformatics/bty459.

Garrido-Sanz, D., Meier-Kolthoff, J.P., Göker, M., Martín, M., Rivilla, R., and Redondo-Nieto, M. (2016). Genomic and genetic diversity within the Pseudomonas fluorescens complex. PLoS One *11*, e0150183. https://doi.org/10.1371/journal.pone.0150183.

Gomez-Valero, L., and Buchrieser, C. (2019). Intracellular parasitism, the driving force of evolution of Legionella pneumophila and the genus Legionella. Genes Immun. *20*, 394–402. https://doi.org/10.1038/s41435-019-0074-z.

Gomila, M., Peña, A., Mulet, M., Lalucat, J., and García-Valdés, E. (2015). Phylogenomics and systematics in Pseudomonas. Front. Microbiol. *6*, 214. https://doi.org/10.3389/fmicb.2015.00214.

Guérin, J., Bigot, S., Schneider, R., Buchanan, S.K., and Jacob-Dubuisson, F. (2017). Two-partner secretion: combining efficiency and simplicity in the secretion of large proteins for bacteria-host and bacteria-bacteria interactions. Front. Cell. Infect. Microbiol. *7*, 148. https://doi.org/10.3389/fcimb.2017.00148.

Huber, P. (2020). Targeting of the apical junctional complex by bacterial pathogens. Biochim. Biophys. Acta Biomembr. *1862*, 183237. https://doi.org/10.1016/j.bbamem.2020.183237.

Jacob-Dubuisson, F., Fernandez, R., and Coutte, L. (2004). Protein secretion through autotransporter and two-partner pathways. Biochim. Biophys. Acta *1694*, 235–257. https://doi.org/10.1016/j.bbamcr.2004.03.008.

Jacob-Dubuisson, F., Guérin, J., Baelen, S., and Clantin, B. (2013). Two-partner secretion: as simple as it sounds? Res. Microbiol. *164*, 583–595. https://doi.org/10.1016/j.resmic.2013.03.009.

Johnson, R.M., Nash, Z.M., Dedloff, M.R., Shook, J.C., and Cotter, P.A. (2021). DegP initiates regulated processing of filamentous hemagglutinin in bordetella bronchiseptica. mBio *12*, e0146521. https://doi.org/10.1128/mBio.01465-21.

Kos, V.N., Déraspe, M., McLaughlin, R.E., Whiteaker, J.D., Roy, P.H., Alm, R.A., Corbeil, J., and Gardner, H. (2015). The resistome of Pseudomonas aeruginosa in relationship to phenotypic susceptibility. Antimicrob. Agents Chemother. *59*, 427–436. https://doi.org/10.1128/AAC.03954-14.

Keel, C. (2016). A look into the toolbox of multi-talents: insect pathogenicity determinants of plant-beneficial pseudomonads. Environ. Microbiol. *18*, 3207–3209. https://doi.org/10.1111/1462-2920.13462.

Koonin, E.V. (2016). Horizontal gene transfer: essentiality and evolvability in prokaryotes, and roles in evolutionary transitions. F1000Research *5*, F1000. https://doi.org/10.12688/f1000research.8737.1.

Kupferschmied, P., Maurhofer, M., and Keel, C. (2013). Promise for plant pest control: root-associated pseudomonads with insecticidal activities. Front. Plant Sci. *4*, 287. https://doi.org/10.3389/fpls.2013.00287.

Lalucat, J., Mulet, M., Gomila, M., and García-Valdés, E. (2020). Genomics in bacterial taxonomy: impact on the genus Pseudomonas. Genes *11*, E139. https://doi.org/10.3390/genes11020139.

Li, M.Z., and Elledge, S.J. (2007). Harnessing homologous recombination in vitro to generate recombinant DNA via SLIC. Nat. Methods *4*, 251–256. https://doi.org/10.1038/nmeth1010.

Liehl, P., Blight, M., Vodovar, N., Boccard, F., and Lemaitre, B. (2006). Prevalence of local immune response against oral infection in a Drosophila/Pseudomonas infection model. PLoS Pathog. *2*, e56. https://doi.org/10.1371/journal.ppat.0020056.

Liu, J.R., Lin, Y.D., Chang, S.T., Zeng, Y.F., and Wang, S.L. (2010). Molecular cloning and characterization of an insecticidal toxin from Pseudomonas taiwanensis. J. Agric. Food Chem. *58*, 12343–12349. https://doi.org/10.1021/jf103604r.

Loewen, P.C., Villenueva, J., Fernando, W.G., and de Kievit, T. (2014). Genome sequence of Pseudomonas chlororaphis strain PA23. Genome Announc. *2*, e00689-14. https://doi.org/10.1128/genomeA.00689-14.

Maier, T., Clantin, B., Gruss, F., Dewitte, F., Delattre, A.S., Jacob-Dubuisson, F., Hiller, S., and Villeret, V. (2015). Conserved Omp85 lid-lock structure and substrate recognition in FhaC. Nat. Commun. *6*, 7452. https://doi.org/10.1038/ncomms8452.

Manuel, J., Selin, C., Fernando, W.G., and de Kievit, T. (2012). Stringent response mutants of Pseudomonas chlororaphis PA23 exhibit enhanced antifungal activity against Sclerotinia sclerotiorum in vitro. Microbiology *158*, 207–216. https://doi.org/10.1099/mic.0.053082-0.

Maretzky, T., Reiss, K., Ludwig, A., Buchholz, J., Scholz, F., Proksch, E., de Strooper, B., Hartmann, D., and Saftig, P. (2005). ADAM10 mediates E-cadherin shedding and regulates epithelial cell-cell adhesion, migration, and beta-catenin translocation. Proc. Natl. Acad. Sci. USA *102*, 9182–9187. https://doi.org/10.1073/pnas.0500918102.

Mazar, J., and Cotter, P.A. (2007). New insight into the molecular mechanisms of two-partner secretion. Trends Microbiol. *15*, 508–515. https://doi.org/10.1016/j.tim.2007.10.005.

Minh, B.Q., Schmidt, H.A., Chernomor, O., Schrempf, D., Woodhams, M.D., von Haeseler, A., and Lanfear, R. (2020). IQ-TREE 2: new models and efficient methods for phylogenetic inference in the genomic Era. Mol. Biol. Evol. *37*, 1530–1534. https://doi.org/10.1093/molbev/msaa015.

Na, S.-I., Kim, Y.O., Yoon, S.-H., Ha, S.m., Baek, I., and Chun, J. (2018). UBCG: up-to-date bacterial core gene set and pipeline for phylogenomic tree reconstruction. J. Microbiol. *56*, 280–285. https://doi.org/10.1007/s12275-018-8014-6.

Nash, Z.M., and Cotter, P.A. (2019a). Bordetella filamentous hemagglutinin, a model for the two-partner secretion pathway. Microbiol. Spectr. *7*. https://doi.org/10.1128/microbiolspec.PSIB-0024-2018.

Nash, Z.M., and Cotter, P.A. (2019b). Regulated, sequential processing by multiple proteases is required for proper maturation and release of Bordetella filamentous hemagglutinin. Mol. Microbiol. *112*, 820–836. https://doi.org/10.1111/mmi.14318.

Notredame, C., Higgins, D.G., and Heringa, J. (2000). T-coffee: a novel method for fast and accurate multiple sequence alignment 1 1. J. Mol. Biol. *302*, 205–217. https://doi.org/10.1006/jmbi.2000.4042.

Oberto, J. (2013). SyntTax: a web server linking synteny to prokaryotic taxonomy. BMC Bioinformatics *14*, 4. https://doi.org/10.1186/1471-2105-14-4.

Opota, O., Vallet-Gély, I., Vincentelli, R., Kellenberger, C., Iacovache, I., Gonzalez, M.R., Roussel, A., van der Goot, F.G., and Lemaitre, B. (2011). Monalysin, a novel ß-pore-forming toxin from the Drosophila pathogen Pseudomonas entomophila, contributes to host intestinal damage and lethality. PLoS Pathog. *7*, e1002259. https://doi.org/10.1371/journal.ppat.1002259.

Organization, W.H. (2019). Guidelines for the Prevention and Control of Carbapenem-Resistant Enterobacteriaceae, Acinetobacter Baumannii and Pseudomonas aeruginosa in Health Care Facilities (World Health Organization).

Peix, A., Ramírez-Bahena, M.H., and Velázquez, E. (2018). The current status on the taxonomy of Pseudomonas revisited: an update. Infect. Genet. Evol. *57*, 106–116. https://doi.org/10.1016/j.meegid.2017.10.026.

Perez-Riverol, Y., Csordas, A., Bai, J., Bernal-Llinares, M., Hewapathirana, S., Kundu, D.J., Inuganti, A., Griss, J., Mayer, G., Eisenacher, M., et al. (2019). The PRIDE database and related tools and resources in 2019: improving support for quantification data. Nucleic Acids Res. *47*, D442–D450. https://doi.org/10.1093/nar/gky1106.

Pukatzki, S., Kessin, R.H., and Mekalanos, J.J. (2002). The human pathogen Pseudomonas aeruginosa utilizes conserved virulence pathways to infect the social amoeba Dictyostelium discoideum. Proc. Natl. Acad. Sci. USA *99*, 3159–3164. https://doi.org/10.1073/pnas.052704399.

Reboud, E., Bouillot, S., Patot, S., Béganton, B., Attrée, I., and Huber, P. (2017). Pseudomonas aeruginosa ExlA and Serratia marcescens ShlA trigger cadherin cleavage by promoting calcium influx and ADAM10 activation. PLoS Pathog. *13*, e1006579. https://doi.org/10.1371/journal.ppat.1006579.

Reboud, E., Elsen, S., Bouillot, S., Golovkine, G., Basso, P., Jeannot, K., Attrée, I., and Huber, P. (2016). Phenotype and toxicity of the recently discovered exlA-positive Pseudomonas aeruginosa strains collected worldwide. Environ. Microbiol. *18*, 3425–3439. https://doi.org/10.1111/1462-2920.13262.

Robinson, O., Dylus, D., and Dessimoz, C. (2016). Phylo.io: interactive viewing and comparison of large phylogenetic trees on the web. Mol. Biol. Evol. *33*, 2163–2166. https://doi.org/10.1093/molbev/msw080.

Ronquist, F., Teslenko, M., van der Mark, P., Ayres, D.L., Darling, A., Höhna, S., Larget, B., Liu, L., Suchard, M.A., and Huelsenbeck, J.P. (2012). MrBayes 3.2: efficient bayesian phylogenetic inference and model choice across a large model space. Syst. Biol. *61*, 539–542. https://doi.org/10.1093/sysbio/sys029.

Ruhe, Z.C., Low, D.A., and Hayes, C.S. (2020). Polymorphic toxins and their immunity proteins: diversity, evolution, and mechanisms of delivery. Annu. Rev. Microbiol. *74*, 497–520. https://doi.org/10.1146/annurev-micro-020518-115638.

Savchuk, S., and Dilantha Fernando, W.G. (2004). Effect of timing of application and population dynamics on the degree of biological control of Sclerotinia sclerotiorum by bacterial antagonists. FEMS Microbiol. Ecol. *49*, 379–388. https://doi.org/10.1016/j.femsec.2004.04.014.

Schneider, C.A., Rasband, W.S., and Eliceiri, K.W. (2012). NIH Image to ImageJ: 25 years of image analysis. Nat. Methods *9*, 671–675. https://doi.org/10.1038/nmeth.2089.

Schwanhausser, B., Busse, D., Li, N., Dittmar, G., Schuchhardt, J., Wolf, J., Chen, W., and Selbach, M. (2011). Global quantification of mammalian gene expression control. Nature *473*, 337–342. https://doi.org/10.1038/nature10098.

Sentausa, E., Basso, P., Berry, A., Adrait, A., Bellement, G., Coute, Y., Lory, S., Elsen, S., and Attree, I. (2020). Insertion sequences drive the emergence of a highly adapted human pathogen. Microb. Genom. ,, *6*. https://doi.org/10.1099/mgen.0.000265.

Silby, M.W., Winstanley, C., Godfrey, S.A., Levy, S.B., and Jackson, R.W. (2011). Pseudomonas genomes: diverse and adaptable. FEMS Microbiol. Rev. *35*, 652–680. https://doi.org/10.1111/j.1574-6976.2011.00269.x.

Simons, J.L., and Vintiner, S.K. (2011). Effects of histological staining on the analysis of human DNA from archived slides. J. Forensic Sci. *56*, S223–S228. https://doi.org/10.1111/j.1556-4029.2010.01595.x.

Simons, K., and Gerl, M.J. (2010). Revitalizing membrane rafts: new tools and insights. Nat. Rev. Mol. Cell Biol. *11*, 688–699. https://doi.org/10.1038/nrm2977.

Sullivan, M.J., Petty, N.K., and Beatson, S.A. (2011). Easyfig: a genome comparison visualizer. Bioinformatics *27*, 1009–1010. https://doi.org/10.1093/bioinformatics/btr039.

Trouillon, J., Sentausa, E., Ragno, M., Robert-Genthon, M., Lory, S., Attrée, I., and Elsen, S. (2020). Species-specific recruitment of transcription factors dictates toxin expression. Nucleic Acids Res. *48*, 2388–2400. https://doi.org/10.1093/nar/gkz1232.

ur Rahman, S., Arenas, J., Öztürk, H., Dekker, N., and van Ulsen, P. (2014). The polypeptide transport-associated (POTRA) domains of TpsB transporters determine the system specificity of two-partner secretion systems. J. Biol. Chem. *289*, 19799–19809. https://doi.org/10.1074/jbc.M113.544627.

Vacheron, J., Péchy-Tarr, M., Brochet, S., Heiman, C.M., Stojiljkovic, M., Maurhofer, M., and Keel, C. (2019). T6SS contributes to gut microbiome invasion and killing of an herbivorous pest insect by plant-beneficial Pseudomonas protegens. ISME J. *13*, 1318–1329. https://doi.org/10.1038/s41396-019-0353-8.

Vallet-Gely, I., Novikov, A., Augusto, L., Liehl, P., Bolbach, G., Pechy-Tarr, M., Cosson, P., Keel, C., Caroff, M., and Lemaitre, B. (2010a). Association of hemolytic activity of Pseudomonas entomophila, a versatile soil bacterium, with cyclic lipopeptide production. Appl. Environ. Microbiol. *76*, 910–921. https://doi.org/10.1128/aem.02112-09.

Vallet-Gely, I., Opota, O., Boniface, A., Novikov, A., and Lemaitre, B. (2010b). A secondary metabolite acting as a signalling molecule controls Pseudomonas entomophila virulence. Cell Microbiol. *12*, 1666–1679. https://doi.org/10.1111/j.1462-5822.2010.01501.x.

Vesga, P., Augustiny, E., Keel, C., Maurhofer, M., and Vacheron, J. (2021). Phylogenetically closely related pseudomonads isolated from arthropods exhibit differential insect-killing abilities and genetic variations in insecticidal factors. Environ. Microbiol. https://doi.org/10.1111/1462-2920.15623.

Vesga, P., Flury, P., Vacheron, J., Keel, C., Croll, D., and Maurhofer, M. (2020). Transcriptome plasticity underlying plant root colonization and insect invasion by Pseudomonas protegens. ISME J. *14*, 2766–2782. https://doi.org/10.1038/s41396-020-0729-9.

Vodovar, N., Vallenet, D., Cruveiller, S., Rouy, Z., Barbe, V., Acosta, C., Cattolico, L., Jubin, C., Lajus, A., Segurens, B., et al. (2006). Complete genome sequence of the entomopathogenic and metabolically versatile soil bacterium Pseudomonas entomophila. Nat. Biotechnol. *24*, 673–679. https://doi.org/10.1038/nbt1212.

Vodovar, N., Vinals, M., Liehl, P., Basset, A., Degrouard, J., Spellman, P., Boccard, F., and Lemaitre, B. (2005). Drosophila host defense after oral infection by an entomopathogenic Pseudomonas species. Proc. Natl. Acad. Sci. USA *102*, 11414–11419. https://doi.org/10.1073/pnas.0502240102.

Weaver, T.M., Hocking, J.M., Bailey, L.J., Wawrzyn, G.T., Howard, D.R., Sikkink, L.A., Ramirez-Alvarado, M., and Thompson, J.R. (2009). Structural and functional studies of truncated hemolysin A from Proteus mirabilis. J. Biol. Chem. *284*, 22297–22309. https://doi.org/10.1074/jbc.M109.014431.

Wiehlmann, L., Cramer, N., and Tümmler, B. (2015). Habitat-associated skew of clone abundance in the Pseudomonas aeruginosa population. Environ. Microbiol. Rep. *7*, 955–960. https://doi.org/10.1111/1758-2229.12340.

Winsor, G.L., Griffiths, E.J., Lo, R., Dhillon, B.K., Shay, J.A., and Brinkman, F.S. (2016). Enhanced annotations and features for comparing thousands of Pseudomonas genomes in the Pseudomonas genome database. Nucleic Acids Res. *44*, D646–D653. https://doi.org/10.1093/nar/gkv1227.

Yang, G., and Waterfield, N.R. (2013). The role of TcdB and TccC subunits in secretion of the Photorhabdus Tcd toxin complex. PLoS Pathog. *9*, e1003644. https://doi.org/10.1371/journal.ppat.1003644.

Yeo, H.J., Yokoyama, T., Walkiewicz, K., Kim, Y., Grass, S., and Geme, J.W.S. (2007). The structure of the Haemophilus influenzae HMW1 pro-piece reveals a structural domain essential for bacterial two-partner secretion. J. Biol. Chem. *282*, 31076–31084. https://doi.org/10.1074/jbc.M705750200.

Zambolin, S., Clantin, B., Chami, M., Hoos, S., Haouz, A., Villeret, V., and Delepelaire, P. (2016). Structural basis for haem piracy from host haemopexin by Haemophilus influenzae. Nat. Commun. *7*, 11590. https://doi.org/10.1038/ncomms11590.

Zhang, D., de Souza, R.F., Anantharaman, V., Iyer, L.M., and Aravind, L. (2012). Polymorphic toxin systems: comprehensive characterization of trafficking modes, processing, mechanisms of action, immunity and ecology using comparative genomics. Biol. Direct *7*, 18. https://doi.org/10.1186/1745-6150-7-18.

STAR★METHODS

KEY RESOURCES TABLE

REAGENT or RESOURCE	SOURCE	IDENTIFIER
Antibodies		
Anti-Flotillin-2 (mouse)	Abnova, Taiwan	Cat# H00002319-M03; RRID:AB_1674827
Anti-E-cadherin Cter	BD Transduction Laboratories	Cat# 610181; RRID:AB_397580
Anti-β-tubulin	Sigma	Cat# T0198; RRID:AB_477556
Anti-mouse-HRP	Sigma	Cat# A9044; RRID:AB_258431
Anti-rabbit-HRP	Sigma	Cat# A9169; RRID:AB_258434
Anti-ExlA-Cter	Biotem	Basso et al. 2017
Anti-ExlA-Nter	Biotem	Berry et al. 2018
Anti-ExlA (3 peptides)	Biotem	Elsen et al. 2014
Bacterial and virus strains		
PAO1	Reference strain, wild type	https://www.pseudomonas.com/strain
IHMA879472	IHMA[1] collection, (Basso et al., 2017; Kos et al., 2015)	urinary infection, ExlA + strain
IHMA87Δ*exlBA*	Trouillon et al. (2020)	Deletion of *exlBA* operon
IHMA87D*exlBA*:: *exlBAPa*	This work	IHMA87 Δ*exlBA* with pSW196-*exlBA*^{Pa} in *attB* site (TcR)
IHMA87D*exlBA*:: *exlBAPa*^{Nter}	This work	IHMA87 Δ*exlBA* with pSW196-*exlBA*$^{Pa\text{-}Nter}$ in *attB* site (TcR)
IHMA87D*exlBA*:: *exlBAPa*^{Nter}*Pe*^{CTD}	This work	IHMA87 Δ*exlBA* with pSW196-*exlBA*$^{Pa\text{-}Nter}$*Pe*^{CTD} in *attB* site (TcR)
IHMA87D*exlBA*:: *exlBAPa*^{Nter}*Pp*^{CTD}	This work	IHMA87 Δ*exlBA* with pSW196-*exlBA*$^{Pa\text{-}Nter}$*Pp*^{CTD} in *attB* site (TcR)
PA23	T. de Kievit, Loewen et al. (2014)	Reference strain, wild type
PA23 Δ*exlBA*	Trouillon et al. (2020)	Partial deletion of *exlBA*
CIP103295T	Institute Pasteur Collection	*subsp. aureofaciens*, isolated from Maas River clay
CIP106718T	Institute Pasteur Collection	*subsp. aurantiaca*
CIP110232T	Institute Pasteur Collection	*subsp. piscium*, isolated from distal intestine of *Perca fluviatilis*
CIP63.22T	Institute Pasteur Collection	*subsp. chlororaphis*, plate contaminant
CIP75.23	Institute Pasteur Collection	Soil isolate
CIP76.23	Institute Pasteur Collection	Isolate from grated carrot
M11740	(Faccone et al., 2014)	Human clinical isolate, Argentina
Pc18-6031	CHU Besançon, France	Human clinical isolate, France
L48	B. Lemaitre, (Vodovar et al., 2006)	Entomopathogen, wild type
L48D*mnl*::INT*exlA*	This work	Double mutant in *mnl* and *exlA* (GmR)
L48D*mnl*	B. Lemaitre, Opota et al. (2011)	Deletion of a gene encoding Monalysin
L48::INT*exlA*	This work	Insertion of pINT in *exlA* gene locus PSEEN2177 (named *exlA*-mut) (Gm^{R})
L48D*gacA*	B. Lemaitre, Vallet-Gely et al. (2010a),2010b	Deletion of *gacA*
L48D*gacA*::INT*exlA*	This work	Double mutant in *gacA* and *exlA* (GmR)
L48Δ*exlBA*	This work	Partial deletion of *exlBA*
L48D*exlBA* + *exlBA*^{Pe}	This work	L48 Δ*exlBA* with pSW196-*exlBA*^{Pe} (TcR)

(*Continued on next page*)

Continued

REAGENT or RESOURCE	SOURCE	IDENTIFIER
L48D*exlBA* + *exlBAPe*^{Nter}	This work	L48 Δ*exlBA* with pSW196-*exlBA*$^{Pe\text{-}Nter}$ (TcR)
L48D*exlBA* + *exlBAPe*^{Nter}*Pa*^{CTD}	This work	L48 Δ*exlBA* with pSW196-*exlBA*$^{Pe\text{-}Nter}$ *Pa*^{CTD} (TcR)
L48D*exlBA* + *exlBAPe*^{Nter}*Pp*^{CTD}	This work	L48 Δ*exlBA* with pSW196-*exlBA*$^{Pe\text{-}Nter}$ *Pp*^{CTD} (TcR)
KT2440	E. Gueguen, Lyon	*P. putida*, reference strain
KT2440 + *exlBA*^{Pp}	This work	KT2440 with pSW196-*exlBA*^{Pp} (Tc^{R}) expressing *exlBA*^{Pp}
163689	Collection of NRC-AR,[2] Besançon, France	*P. asiatica* Human clinical isolate, France
164217	Collection of NRC-AR,[2] Besançon, France	*P. plecoglossicida* Human clinical isolate, France
174639	Collection of NRC-AR,[2] Besançon, France	*P. putida* Human clinical isolate, France
174761	Collection of NRC-AR,[2] Besançon, France	*P. monteilii* Human clinical isolate, France
185589	Collection of NRC-AR,[2] Besançon, France	*P. monteilii* Human clinical isolate, France
185733	Collection of NRC-AR,[2] Besançon, France	*P. putida* Human clinical isolate, France
185840	Collection of NRC-AR,[2] Besançon, France	*P. monteilii* Human clinical isolate, France
185886	Collection of NRC-AR,[2] Besançon, France	*P. mosselii* Human clinical isolate, France
186043	Collection of NRC-AR,[2] Besançon, France	*P. putida* Human clinical isolate, France
TOP10	Invitrogen	Laboratory strain used for cloning
Biological samples		
Fetal Calf serum	Thermo Scientific	Cat# 10270-106
Chemicals, peptides, and recombinant proteins		
NuPAGE LDS sample buffer 4x	Thermo Scientific	Cat# 2201423
Reducing Agent 10x	Thermo Scientific	Cat# 221429
4-20% NuPAGE Tris-Glycine	Thermo Scientific	Cat# NP0321BOX
Protease inhibitor cocktail	Roche	Cat# 11873580001
Triton X-100	Sigma	Cat# T8787-100mL
Sequencing Grade Modified Trypsin	Promega	Cat# V5111
LB Broth Miller Luria Bertani	BD Diagnostic	Cat# 244610
LB Agar Miller Luria Bertani	BD Diagnostic	Cat# 244510
Rifampycin	Sigma	Cat# R3501-1G
Tetracyclin	Sigma	Cat# T7660-25G
Gentamycin	Sigma	Cat# G1264-5G
Irgasan	Sigma	Cat# 72779-25G-F
DMEM	Life Technology	Cat# 10567014
Propidium iodide	Life Technology	Cat# P4864
Arabinose	Sigma	Cat# A3256-100G
PBS	Euromedex	Cat# ET330-A
EDTA	Sigma	Cat# ED2SS-50G
Sodium Orthovanadate	Sigma	Cat# 5086050001
Okadaic acid	Sigma	Cat# 495604-25UG
Acrylamide-Bisacrylamide	Euromedex	Cat# EU0074-B
PVDF membrane 0.2µm	Amersham Hybond	Cat# 10600021
R250 Coomassie blue	BioRad	Cat# 1610400
HEPES	Sigma	Cat# H3375
EGTA	Sigma	Cat# E4378
NaCl	Sigma	Cat# 71383

(*Continued on next page*)

Continued

REAGENT or RESOURCE	SOURCE	IDENTIFIER
Glucose	Sigma	Cat# G5767-500G
Saccharose	Sigma	Cat# S0389
NUPAGE 4-12% BisTris	Thermo Scientific	Cat# WG1402BOX
MOPS	Sigma	Cat# M1254-250G
PYG medium	Eurobio	Cat# PYG-500
TBS	Euromedex	Cat# ET220
Critical commercial assays		
Cell Surface Biotinylation and Isolation kit	Thermo Fisher Scientific	Cat# A44390
Micro BCA Protein Assay Kit	Thermo Fisher Scientific	Cat# 23235
Deposited data		
Proteomic data	This paper	Dataset identifier PXD029397 on www.proteomexchange.org
Experimental models: Cell lines		
Epithelial cells A549	ATCC	ATCC CCL-185
Macrophages cells J774A-1	ATCC	ATCC BIT67
Experimental models: Organisms/strains		
Drosophila melanogaster		genotype w^{1118} in a Canton-S genetic background
Galleria mellonella	Sud-Est Appats	http://www.sudestappats.fr
Acanthamoeba castellanii	ATCC	ATCC 1034
Software and algorithms		
ImageJ	Schneider et al., 2012	https://imagej.nih.gov/ij/
Adobe Illustrator CS6	Adobe	https://www.adobe.com/ca/products/illustrator.html
SIAS tool	Reche et al., 2008 - Universidad Complutense de Madrid Facultad de Medicina Departamento de Immunología (Microbiología I)	http://imed.med.ucm.es/Tools/sias.html
SyntTaxtool	Oberto, 2013	http://archaea.u-psud.fr/SyntTax
Easyfig 2.2.2 software	Sullivan et al., 2011	https://mjsull.github.io/Easyfig/
UBCG pipeline	Na et al., 2018	https://www.ezbiocloud.net/tools/ubcg
Probcons software	Do et al., 2005	http://probcons.stanford.edu/download.html
T-coffee	Notredame et al., 2000	https://www.tcoffee.org/Projects/tcoffee/index.html#DOWNLOAD
IQ-TREE 2	Minh et al., 2020	http://www.iqtree.org/
Prottest software	Darriba et al., 2011	https://github.com/ddarriba/prottest3
Mr Bayes 3.2.6	Ronquist et al., 2012	https://nbisweden.github.io/MrBayes/download.html
FigTreev1.4.3	FigTree	http://tree.bio.ed.ac.uk/software/figtree/
Mascot	Matrix Science	https://www.matrixscience.com/cgi/search_form.pl?FORMVER=2&SEARCH=PMF
Xcalibur	Thermo Fisher Scientific	Xcalibur™ Software - OPTON-30965
Proline	Bouyssié et al., 2020	https://www.profiproteomics.fr/proline/
Sigma Plot	Jandel Scientific	https://systatsoftware.com/sigmaplot

[1]International Health Management Association, USA.
[2]National Reference Center for Antibiotic Resistance.

RESOURCE AVAILABILITY

Lead contact

Further information and requests for resources and reagents should be directed to and will be fulfilled by the lead contact, Ina Attrée, ina.attree@ibs.fr.

Materials availability

This study did not generate new unique reagents or insect lines.

Plasmids and bacterial strains generated in this study are available from the lead contact.

Data and code availability

The scripts used in this study are available upon request to the lead contact.

Any additional information required to reanalyze the data reported in this paper is available from the lead contact upon request.

The mass spectrometry proteomics data have been deposited in the ProteomeXchange (www.proteomexchange.org) with the unique dataset identifier PXD029397 also reported in the key resources table.

EXPERIMENTAL MODEL AND SUBJECT DETAILS

Bacterial strains and culture cell conditions

P. chlororaphis PA23 (Loewen et al., 2014) was a gift from Terasa de Kievit, University of Manitoba, Canada. *P. aeruginosa* IHMA87 is an isolate from a urinary tract infection and was previously shown to secrete Exolysin (Elsen et al., 2014). *P. putida* KT2440 was obtained from the laboratory UMR5240, Lyon, France. *P. entomophila* L48 (Vodovar et al., 2005) and derivatives were obtained from Bruno Lemaitre's lab (EPFL, Switzerland). Bacteria were grown in liquid LB medium (Becton Dickinson) at 28-30°C (for *P. entomophila*, *P. putida* and *P. chlororaphis*) or 37°C (for *P. aeruginosa*) with 300 rpm agitation. After overnight incubation, strains were diluted in LB medium to reach optical density measured at 600_{nm} (OD_{600}) of 1.0 at 30°C or 37°C, respectively. When needed, arabinose (0-0.5%, as indicated) was added to the growing cultures in LB, and tetracycline 10 μg/mL was always added in LB and DMEM for *P. putida* and *P. entomophila* cultures to maintain the replication of pSW196.

Epithelial lung carcinoma cell line A549 (ATCC CCL-185) and J774 macrophages were grown in DMEM (Life Technologies) supplemented with 10% fetal calf serum (Lonza). For cytotoxicity test, cells were seeded at $1{,}25 \times 10^4$ cells per well for A549 and 10^5 cells per well for J744 on black μclear 96-well plates (Greiner) and used 48 h later to obtain confluent monolayers. One hour before infection, medium was replaced by DMEM without phenol red, supplemented with propidium iodide (PI, Sigma, 1 μM). For lipid raft experiments, epithelial cell line A549 was seeded in four 94-mm Petri dish at one or 2×10^7 cells/dish and infected in 6 mL of fresh DMEM media. While for membrane purification only one 94-mm Petri dish was used. Cells were infected with bacterial cultures grown until OD_{600} of 1 (for *P. aeruginosa*, *P. putida* and *P. chlororaphis*) or overnight culture (for *P. entomophila*) at a MOI of 10. Infections were performed in presence of 5% CO_2 at 37°C for *P. aeruginosa* or at 30°C for *P. entomophila*, *P. chlororaphis* and *P. putida* + pSW196-*exlBA*^{Pp}. For *P. putida* 0.5% arabinose was added in the bacterial culture and 0.1% in the infection dish to ensure ExlA expression. For all experiments infections were monitored by microscopy and stopped when approximately 60-70% of the cells started to change the morphology and shrink (in the case of *P. aeruginosa* and *P. chlororaphis*), or when >60% cells were IP positive in a control plate for infection with *P. entomophila* and *P. putida*.

Acanthamoeba castellanii (ATCC 1034) was cultured at 30°C in flasks with 20 mL of PYG medium (2% proteose peptone, 0.1%, yeast extract, 0.1% sodium citrate dihydrate, 0.4 mM $CaCl_2$, 4 mM $MgSO_4$, 2.5 mM Na_2HPO_4, 2.5 mM KH_2PO_4, 0.05 mM $Fe(NH_4)_2(SO_4)_2$, 0.1 M Glucose).

Drosophila and *Galleria*

Drosophila melanogaster flies (genotype w^{1118} in a Canton-S genetic background) were maintained at 25°C on standard yeast-containing fly medium. For oral infection we used 4- to 8-day old females, while acute infection was done on 7- to 10-day old female flies.

Galleria mellonella were purchased from Sud-Est Appats (73720 Queige, France) and held at room temperature until used within two days maximal. Twenty randomly selected larvae were transfer in Petri dish and used per group.

METHOD DETAILS

Genetic constructions

The plasmid used to inactivate the PSEEN2177 gene (*exlA*^{Pe}) was a gift from Isabelle Vallet-Galey (I2BC-CNRS, Paris, France) and was used to construct the *exlA*^{Pe} mutant (named *exlA-mut* in the main text). The strain was verified by PCR and sequencing for transposon insertion. For the *P. chlororaphis* PA23 Δ*exlBA* (*RS20945/950*) mutant construct, a 900 bp fragment containing a deletion was synthesized by Genewiz and subcloned in *Eco*RI-*Hin*dIII of pEXG2, leading to pEXG2-Mut-Pchloro_*exlBA*. To obtain the deletion of the *P. entomophila exlBA* operon, the pEXG2-Pe_Δ*exlBA* was obtained by sequence and ligation–independent cloning (SLIC) (Li and Elledge, 2007) using primers described in Table S5. The plasmids were transferred into *P. chlororaphis* or *P. entomophila* by triparental mating using pRK600 as a helper plasmid. For allelic exchange, cointegration events were first selected on LB plates containing rifampicin (25 μg/mL) and gentamicin (25 μg/mL) at 28°C. Single colonies were then plated on NaCl-free LB agar plates containing 10% (wt/vol) sucrose to select for the loss of plasmid. The sucrose-resistant strains were checked for gentamicin sensitivity and mutant genotype by PCR. For heterologous expression of *exlBA* operons of *P. entomophila* and *P. putida*, the operons were synthetized by Genewiz and cloned in pSW196 harboring arabinose-inducible promoter (Baynham et al., 2006). The *P. entomophila* operon *exlBA*^{Pe} (*PSEEN2177*/*PSEEN2176*) was synthetized as an *Eco*RI-*Spe*I fragment with a putative RBS of *exlBA* from *P. aeruginosa* PA7 (gatacatgaaggatgccgc). Additional *Avr*II (cctagg) restriction site was created around the codon for Leu^{1294}, just at the beginning of the C-terminal domain (starting from Ala^{1296}), without change of the amino acid sequence. This *Avr*II site will be further used for the construction of the C-terminal domain deletion mutant (ExlA$^{Pe-Nter}$) (by introducing the Ala1296Stop mutation) and the chimeric proteins. The *P. putida* operon (*PP_1450/PP_1449*) was synthetized as an *Eco*RI–*Sac*I fragment with the putative RBS of *exlBA* from *P. aeruginosa* PA7, this first construct pSW196-*exlBA*^{Pp}* did not expressed ExlA after arabinose induction. In this construct the RBS was positioned in front of *exlB* starting from TTG (Met^{1}) in agreement with annotation at http://pseudomonas.com (Winsor et al., 2016). As the second Met, just five amino acids apart, could also serve as a start codon, we deleted by site-directed mutagenesis the sequence encoding the first 5 residues (MRGAS). The resulting pSW196-*exlBA*^{Pp} showed good expression and secretion of ExlA after arabinose induction. The operon sequences were verified by sequencing.

Protein chimeras were designed to exchange the CTD of ExlA^{Pa} with the *Pe*^{CTD} and *Pp*^{CTD}, and the CTD of ExlA^{Pe} was exchanged by the *Pa*^{CTD} and *Pp*^{CTD}. Briefly, the sequence of each CTD was amplified by PCR containing an additional 15-bp flanking region corresponding to the pSW196 vector cleaved with *Avr*II and *Spe*I (for the *exlA*^{Pe} chimeras) or *Sac*I and *Srg*DI (for the *exlA*^{Pa} chimeras). Subsequently the PCR products were directly used as templates for SLIC to generate the four pSW196-*exlBA* constructs (Table S1). Primers are listed in Table S5.

All the genetic constructs (pSW196) were introduced into *Pseudomonas* strains by triparental mating using pRK2013 or pRK600, as a helper plasmid. Transconjugants were selected on LB plates supplemented with 25 μg/mL irgasan and 75 μg/mL tetracycline (for *P. aeruginosa*), 25 μg/mL rifampicin and 40 μg/mL tetracycline (for *P. entomophila*) and 25 μg/mL irgasan and 25 μg/mL tetracycline (for *P. putida*).

Cytotoxicity assays and microscopy

Cells were infected at a multiplicity of infection (MOI) of 10, unless otherwise specified. PI incorporation was followed by fluorescence measuring (excitation 544 nm/emission 590 nm) every 10 min with Fluoroskan Ascent FL2.5 Microplate Fluorometer (Thermo Corporation), over indicated time post-infection. Data were presented as arbitrary fluorescence units (AU) as a function of time. Cytotoxicity assays of strains carrying chimeric proteins were performed over 10 h at 30°C for *P. entomophila* in presence of 0.01% arabinose or 37°C for *P. aeruginosa* without arabinose. For comparison between strains, the data were presented as area under the curve (AUC) calculated according to the linear trapezoidal rule, expressed in arbitrary units (AU).

For microscopy, infections were done as described above and images were captured at the end of infection on a LEICA DMIRE2 microscope with an ORCA-05G camera and with an N PLAN x20 numerical aperture 0.40 objective in transmission light and TRITC channel.

E-cadherin cleavage

A549 epithelial cells were seeded on a 6-well plate in the same conditions as previously described. When about 70% of cells were considered as dead, culture medium was removed, cells were lysed with a lysis buffer (PBS 1x, 1 mM EDTA, 1% Triton X-100, Protease inhibitors (Roche), 1 mM orthovanadate and 50 nM okadaic acid) and scrapped. The suspension was centrifuged at 15,000 g during 15 min at 4°C and the supernatant was recovered. Protein concentrations of the lysates were determined with Micro BCA Protein Assay (Thermo Scientific™) using BSA as standard. Proteins (20 μg sample) were separated by a 10% acrylamide gel, then transferred on to a PVDF membrane and revealed with E-cadherin (BD transduction laboratories) or β-actin (Sigma) antibodies. Quantification of the bands was made with ImageJ software, the amount of E-cadherin full-length was normalized to the amount of β-actin and expressed as percentage referred to non-infected condition, considered as 100%.

Lipid raft isolation and western blotting

At the end bacterial infection, lipid raft fractions were purified as follows (Bertrand et al., 2020). Cells were washed twice with 10 mL PBS, then scraped into 400 μL of 50 mM HEPES (pH 7.4), 150 mM NaCl, 5 mM EGTA, 1% Triton X-100 containing a protease inhibitor cocktail (PIC, Roche). Scraped cells were incubated on ice for 1h with frequent vortexing. Finally, cells debris were removed by centrifugation at 1 000 g for 10 min and solubilized materials were applied on the bottom of a centrifuge tube and a sucrose gradient was applied on the top (typically 4 mL of 40% of sucrose containing the soluble fraction, followed by 5 mL of 30% sucrose and 3 mL of 5% sucrose). Lipid rafts appear as a white cloudy bands below the 5% sucrose after ultracentrifugation at 40,000 rpm for 16 h at 4°C using swinging-bucket SW41 Ti rotors. Fractions of 1 mL were recovered from the top to the bottom of each tube and loaded on a gradient 4-12% Bis-Tris Gel (BioRad or Thermo Fisher Scientific). For Western Blot analysis, the proteins were transferred onto a PVDF membrane and incubated with different antibodies. A mixture of rabbit polyclonal anti-ExlA antibodies composed by antibodies against three synthetic peptides designed from the ExlA sequence (dilution 1:500) (Elsen et al., 2014), antibodies anti-ExlA-Cter and anti-ExlA-Nter both diluted 1:1 000 [10]; for *P. entomophila* and *P. putida* experiments only the antibodies anti-ExlA-Nter were used. Mouse antibodies anti-Flotillin-2 (BD Biosciences) were used as lipid raft marker at a dilution of 1:10000 and E-cadherin Cter (36/E-Cadherin, BD Transduction Laboratories) (1:5000) were used as membrane marker. Secondary antibodies anti-mouse-HRP (SIGMA) and anti-rabbit-HRP (SIGMA) were diluted (1:10000) and (1: 50000), respectively.

Cytoplasmic membranes purifications

A549 cytoplasmic membranes were purified following the Pierce™ Cell Surface Protein Biotinylation and Isolation kit protocol (Thermo Fisher Scientific). When more than 70% of the cells showed shrinkage (for *P. aeruginosa* and *P. chlororaphis*) or were IP positive (for *P. entomophila* and *P. putida*), cells were washed with 20 mL PBS and then incubated for 30 min at 4°C in 10 mL of Sulfo-NHS-SS-Biotin solution (all provided in the kit). Labeling solution was then removed and cells were first washed with 20 mL TBS-ice cold twice, then scraped in 20 mL of TBS-ice cold and finally centrifuged 3 min at 500 g. Cells pellet were resuspended into 500 μL lysis buffer (from the kit) containing protease inhibitors (Roche) and incubated 30 min on ice. The cell lysates were centrifuged at 15,000 rpm for 15 min at 4°C, the clarified supernatants (containing solubilized membranes and soluble proteins) were incubated with 250 μL NeutrAvidin Agarose (from the kit) for 30 min at room temperature on a rocking platform. Resins were washed 4 times with 500 μL wash buffer (from the kit), then biotinylated membrane proteins captured on the resin were eluted after incubation for 30 min at room temperature with 200 μL of Elution Buffer containing 10 mM DTT. For immunoblotting, 20 μL of fractions from each step were mixed with NuPAGE LDS sample buffer 4x (Thermo Scientific) and Reducing Agent 10x (Thermo Scientific), heated at 70°C for 10 min and loaded on a 4-20% NuPAGE Tris-Glycine (Thermo Scientific) run in MOPS 1x buffer. Proteins were transferred onto PVDF membrane, blocked overnight at 4°C in 5% non-fat dairy milk before revelation with polyclonal rabbit anti-ExlA-Nter antibodies (dilution 1:1,000) (Basso et al., 2017; Berry et al., 2018). Monoclonal mouse E-cadherin-Cter (36/E-Cadherin, BD Transduction Laboratories) (1:5000) and monoclonal mouse anti-β-tubulin (SIGMA) (1:5000) antibodies were used to develop membrane or cytoplasm markers, respectively. Secondary antibodies anti-mouse-HRP (SIGMA) and anti-rabbit-HRP (SIGMA) were used at 1: 50000 dilution.

Amoeba growth by plaque formation assay

100 μL of overnight bacterial culture were pelleted by centrifugation at 4000 rpm for 5 min and resuspended in 1 mL of M63 medium. 100 μL of this resuspension at OD_{600nm} of 0.1 were spread on M63 Glucose

0.2% agar plates to form a bacterial lawn. The plates were dried 20 min. Amoeba's cells were collected by centrifugation, washed once with M63 medium, and different numbers of amoebae cell in 5 μL M63 were deposited on the top of the agar plate. Plates were incubated at 30°C for 5 days. The least number of *Acanthamoeba castellanii* cells deposited above that was able to form plaque on the bacterial lawns was defined as the minimum number of cells required for plaque formation in this study.

Galleria mellonella infection

Infections of *Galleria* larvae were done as described (Sentausa et al., 2020) with some modifications. The bacterial dose of approx. 6×10^5 bacteria/injection was evaluated in preliminary experiment as such to obtain larval mortality within 40 h post-pricking. 10 μL of bacterial in PBS solution were injected in the larvae using an insulin pen. Incubations were done at 30°C and larvae were counted every 45 min. The death was evaluated by the insusceptibility to touch with plastic tweezers. The dead larvae were removed from the dish. The experiment was repeated at least twice.

Drosophila infections

For oral infection flies were starved in an empty vial before their transfer to a contaminated vial containing the bacterial or uninfected solutions. *P. chlororaphis* PA23 (wild-type and the Δ*exlBA* mutant) and *P. entomophila* L48 wild-type, Δ*gacA*, Δ*mnl* and the corresponding *exlA* mutant were grown in LB at 28-30°C. Overnight bacterial cultures were pelleted and suspended into a sterile 1% sucrose solution and adjusted to an OD_{600} of 100 corresponding to 1.4 and 6×10^{10} bacteria/mL for *Pe* and *Pch*, respectively. 200 μL of bacterial suspension were added to a filter paper disk placed on the top of a standard fly-feeding medium in the infected vials. Flies were then maintained at 29°C and the survival was monitored over 2 weeks. Vials containing filter paper imbedded with 200 μL 1% sucrose alone were used as negative control. Infection experiment was performed with 40–50 flies per conditions tested distributed as 10 flies per vial.

For acute infection, flies were pricked with a thin needle previously dipped into the bacterial cultures prepared from the exponential phase of growth, pelleted and suspended into a sterile PBS solution and adjusted to an OD_{600} of 20. The flies were anesthetized using CO_2 and placed on a CO_2 pad. The needle was dipped into a drop of the diluted bacteria and the flies were pricked in the upper part of thorax (Fauvarque et al., 2002). A drop of PBS was used as a negative control. Flies were maintained at 29°C and the survival was monitored over 15 h. 50 flies were pricked per conditions tested and distributed by set of 10 flies per vial.

Evolutionary analyses

The amino acid identity between ExlA/B from different species/strains of *Pseudomonas* was calculated using both, the SIAS tool with default parameters (http://imed.med.ucm.es/Tools/sias.html) and blastp comparison analyses. The synteny conservation of the genomic regions containing *exlA/B* was analyzed on selected strains using both the SyntTax webserver (Oberto, 2013) and EasyFig 2.2.2 (Sullivan et al., 2011). All completely sequenced *Pseudomonas* genomes (690) were downloaded from both NCBI (https://www.ncbi.nlm.nih.gov/genome/) and the *Pseudomonas* genome database (https://www.pseudomonas.com/) (Table S6). We detected both *exlA* and *exlB* homologous in 191 genomes that were then selected for further analyses (Sheet 2, Table S6). First, a species tree of *Pseudomonas* species/strains containing *exlAB* was constructed using these 191 *Pseudomonas* genomes and two *Burkholderia cepacia* genomes that were selected as outgroups for constructing the phylogeny. The tree reconstruction was based on 92 concatenated housekeeping genes and was built with UBCG (Na et al., 2018), which uses MAFFT to create the multi-gene alignment and FastTree for computing the tree. Using the extracted ExlA and ExlB sequences from each genome, we carried out phylogenetic reconstruction of these two proteins. The sequence of each protein was aligned using PROBCONS (Do et al., 2005) and poorly aligned positions were filtered using T-coffee (v.11) (Notredame et al., 2000) to keep only positions with scores between 8 and 9. The resulting alignment was used for phylogenetic reconstruction with two methods: maximum likelihood and bayesian inference. Maximum likelihood phylogenetic trees were reconstructed using IQ-TREE 2 (v2.1.1) (Minh et al., 2020) with the amino acid substitution model selected with ProtTest (Darriba et al., 2011) based on the smallest Akaike Information Criterion. Branch supports were estimated by means of 1,000 ultrafast bootstrap approximation replicates. Likelihood trees were also re-done adding ShlBA proteins from *Serratia marcescens*. Bayesian analyses were conducted with MrBayes 3.2.6 (Ronquist et al., 2012). Two independent runs with 12 chains each were calculated simultaneously for 1 million

generations, sampling every 10 generations. The average standard deviation of split frequencies below 0.01 was used to ensure convergence of the runs. The probability values were generated after discarding the first 25% of the sampled trees. Phylogenetic trees were visualized using Figtree (v1.4.3, http://tree.bio.ed.ac.uk/software/figtree/).

QUANTIFICATION AND STATISTICAL ANALYSIS

Statistics

All statistical analyses were performed using SigmaPlot software. For cytotoxicity on A549 with chimera proteins a one-way ANOVA followed by a Holm-Sidak test was performed. For survival experiments with *Galleria* and *Drosophila*, a log rank statistic method was used.

Mass spectrometry-based quantitative proteomic analysis of secretomes

Overnight cultures of *P. chlororaphis* or *P. entomophila* done in triplicates were centrifuged 10 min at 13,000 rpm at 4°C to separate bacterial cells from secretomes. Laemmli denaturing buffer was added to secretomes followed by a denaturation step by heating for 10 min at 100°C. Samples were analyzed by silver staining on SDS-PAGE (TGX precasted 8-16% acrylamide gels, BioRad). For mass spectrometry, the proteins solubilized in Laemmli buffer were stacked in the top of a 4-12% NuPAGE gel (Invitrogen). After staining with R-250 Coomassie Blue (Biorad), proteins were digested in-gel using trypsin (modified, sequencing purity, Promega), as previously described (Casabona et al., 2013). The resulting peptides were analyzed by online nanoliquid chromatography coupled to MS/MS (Ultimate 3000 RSLCnano and Q-Exactive HF, Thermo Fisher Scientific) using a 140-min gradient. For this purpose, the peptides were sampled on a precolumn (300 μm × 5 mm PepMap C18, Thermo Scientific) and separated in a 75 μm × 250 mm C18 column (Reprosil-Pur 120C18-AQ, 1.9 μm, Dr. Maisch). The MS and MS/MS data were acquired by Xcalibur (Thermo Fisher Scientific). Peptides and proteins were identified by Mascot (version 2.6.0, Matrix Science) through concomitant searches against the NCBI database (*Pseudomonas chlororaphis* strain PA23 taxonomy, June 2020 download) or the Microscope (Medigue et al., 2019) database (*Pseudomonas entomophila* L48 taxonomy, January 2020 download), a homemade database containing the sequences of classical contaminant proteins found in proteomic analyses (human keratins, trypsin, etc.), and the corresponding reversed databases. Trypsin/P was chosen as the enzyme and two missed cleavages were allowed. Precursor and fragment mass error tolerances were set respectively at 10 and 20 ppm. Peptide modifications allowed during the search were: Carbamidomethyl (C, fixed), Acetyl (Protein N-term, variable) and Oxidation (M, variable). The Proline software (Bouyssié et al., 2020) was used for the compilation, grouping, and filtering of the results (conservation of rank 1 peptides, peptide length $\geq$6 amino acids, peptide score $\geq$25, allowing to reach a false discovery rate of peptide-spectrum-match identifications <1% as calculated on peptide-spectrum-match scores by employing the reverse database strategy, and minimum of one specific peptide per identified protein group). Proline was then used to perform a compilation, grouping and MS1 label-free quantification of the identified protein groups based on razor and specific peptides. The results were manually curated to invalidate peptides belonging to deleted or mutated genes that were erroneously detected in the dataset. Intensity-based absolute quantification (iBAQ) (Schwanhausser et al., 2011), values were calculated from MS1 intensities of razor and specific peptides. The iBAQ values were normalized by the sum of iBAQ values in each sample, before averaging the values of the three replicates to generate the final iBAQ value of each sample type. MS data have been deposited to the ProteomeXchange Consortium via the PRIDE partner repository (Perez-Riverol et al., 2019) with the dataset identifier PXD029397.